Oxygen Stiochiometry Effect on Magnetic Properties of $YBa_2Cu_3O_{7-\delta}$ Superconductor

by

Astra Agus Pramana Dasa-Nova

A Thesis Presented to the

FACULTY OF THE COLLEGE OF GRADUATE STUDIES

KING FAHD UNIVERSITY OF PETROLEUM & MINERALS

DHAHRAN, SAUDI ARABIA

In Partial Fulfillment of the
Requirements for the Degree of

MASTER OF SCIENCE

In

PHYSICS

December, 1995

OXYGEN STOICHIOMETRY EFFECT ON MAGNETIC PROPERTIES OF $YBa_2Cu_3O_{7-\delta}$ SUPERCONDUCTOR

BY

ASTRA AGUS PRAMANA DASA-NOVA

A Thesis Presented to the

FACULTY OF THE COLLEGE OF GRADUATE STUDIES

KING FAHD UNIVERSITY OF PETROLEUM & MINERALS

DHAHRAN, SAUDI ARABIA

In Partial Fulfillment of the
Requirements for the Degree of

MASTER OF SCIENCE

In

PHYSICS

DECEMBER 1995

King Fahd University of Petroleum and Minerals
Dhahran, Saudi Arabia
College of Graduate Studies

This thesis written by Astra Agus Pramana DN under the direction of his thesis advisor and approved by his thesis committee, has been presented to and accepted by the Dean, College of Graduate Studies, in partial fulfillment of the requirements for the degree of Master of Science in Physics.

Thesis Committee :

Dr. Khalil A. Ziq (Chairman)

Dr. Hamdan Nasser (Member)

Dr. Hoccine Bahlouli (Member)

Dr. Abdulaziz S. Al-Harthi (Member)

Approved by:

Dr. Muhammad A. Garwan
Department Chairman

Dr. Ala H. Al-Rabeh
Dean, College of Graduate Studies

Date: December , 1995

Dedicated to
My Beloved Parents,

...My Lord, bestow on them Thy Mercy
even as they cherished me in childhood...

ABSTRACT

Magnetic hysteresis loops measurements on single crystal and polycrystalline $YBa_2Cu_3O_x$ high-T_c ceramic reveals that the energy losses increase with the maximum cycling field, in clear disagreement with behavior expected from Bean's model. The magnetic energy losses in Field Cooled (FC) state is observed to be lower than energy losses in Zero Field Cooled (ZFC) state, reflecting that the FC state is a more ordered state.

The remanent magnetization, initially increases rapidly then approaches saturation gradually. For single crystal, the energy losses and the remanant magnetization along the c-axis have been observed to be greater than in the ab-plane.

Upon varying the oxygen content (x) in polycrystalline $YBa_2Cu_3O_x$, the energy losses increases with increasing x, reaching a maximum near x= 6.64 then decreases upon further increase of oxygen content. Calculation of critical current density (J_c) using hysteresis loop and Bean's model, reveals that J_c increasing linearly with oxygen content.

خلاصة

تستعرض هذه الاطروحه قياس تغير المغناطيسيه لمادة $YBa_2Cu_3O_x$ (أحادية البلورة وعديدة البلورات) المفرطه الموصليه ذات درجة الحرارة عاليه لانتقال الطور تنبي هذه الدراسة عن إزدياد في الطاقة المفقودة بازدياد قيمه المجال المغناطيسي وذلك في تغاير واضح لنموذج (Bean). وجدنا أن الطاقة المفقودة في حالة المادة الناتجة عن تبريد العينه بوجود المجال المغناطيسي(FC) تكون أقل من الطاقة المفقودة عند تبريد العينة بدون تأثير المجال المغناطيسي (ZFC) . وهذا يعني أن الحالة (FC) ذات تركيب مغناطيسي أكثر إنتظاماً من حالة (ZFC) .

بدايةً تزاد المغناطيسيه المتبقيه باضطراد ثم تقترب من حالة التشبع تدريجياً. وقد وجدنا أن المغناطيسيه المتبقيه والطاقة المفقوده في اتجاه – c – البلوري تكونان أعلى من القيم المناظرة في المستوى – ab – البلوري .

بتغيير نسبة الاوكسجين (x) في المادة $Y\ Ba_2\ Cu_3\ Ox$ (عديده البلورات) وجد أن الطاقه المفقوده تزداد بإزدياد x حيث تصل إلى قيمه عظمى عند $x = 6.46$ ثم تبدأ بالانخفاض مع ازدياد x . كما وجد أن كثافة التيار الحرج (Jc) . تزداد خطياً مع زيادة x .

Acknowledgment

Praise Allah, Most Merciful, Most Gracious, the Almighty, for giving me the help and guidance that enabled me to accomplish this work succesfully. Salutation is due to the noble prophet, Muhammad, peace and blessing of Allah be upon him.

First of all, I wish to express my deepest, sincere gratitude and appreciation to my thesis advisor, Dr. Khalil A.Ziq for his invaluable supports and guidance throughout this project. Long working hours spent on many week ends and week days should also be remembered. I also wish to acknowledge my thesis comittee: Dr.Hocine Bahlouli, Dr.Abdulaziz Al-Harthi, and especially to Dr.Nasser Hamdan, for countless discussions and critical comments of the manuscript.

Cooperation and assistance extended to me by the faculties, staff, and graduate students of Physics Dept. are greatly acknowledged. Special thanks are due to Dr. M. Faiz for providing the single crystal samples, to Dr. J. Shirokoff for helpful discussions and comments on the manuscript, and to Mr. Kalman Gergely and Mr. Abdullah Bashrawi of Cryogenic Plant of Physics Dept. for providing me the liquid nitrogen and liquid helium during the experiments.

The contribution of my family towards the completion of this project is limitless. They kept inserting my name in their prayers. Ibrahim Abba and many other friends to name but a few, all contributed each in his own way, their help is greatly acknowledged.

Finally, I acknowledge King Fahd University of Petroleum and Minerals for fully supporting this research.

Contents

Abstract (English) iii

Abstract (Arabic) iv

Acknowledgment. v

1 Introduction **1**

1.1 High Temperature Superconductor 4

1.2 Oxygen Stoichiometry & The Ordering Problem in $YBa_2Cu_3O_x$ . . . 5

1.2.1 The Structure 5

1.2.2 Stoichiometry Effects 7

1.2.3 Order Disorder Phenomena 10

1.3 Magnetization Measurements 11

1.3.1 The Meissner Effect 11

1.3.2 The Irreversibility Line 12

1.3.3 Hysteresis Loops 14

1.3.4 Field Cooling and Zero Field Cooling 16

1.4 Motivation 16

2 Experimental Procedures **18**

2 Experimental Procedures 18

2.1 Magnetization Measurement 18

2.1.1 Vibrating Head and Sample Holder 19

2.1.2 Variable Temperature Cryostat 20

2.1.3 Temperature Controller 23

2.1.4 Power Supply and its controller 24

2.1.5 Quenching Station 25

2.2 Sample Preparation 27

2.2.1 Preparation of Different Oxygen Content and Disorder Samples 29

2.3 Basic Experimental Algorithm 32

3 Critical Current Density 33

3.1 Introduction 33

3.2 Results and Analysis 37

3.2.1 Single Crystal Critical Current Density 38

3.2.2 Polycrystalline Critical Current Density 42

4 Energy Losses 52

4.1 Introduction 52

4.2 Results and Analysis 57

4.2.1 Energy losses in $YBa_2Cu_3O_{7-\delta}$ single crystal 57

4.2.2 Energy Losses in Polycrystalline $YBa_2Cu_3O_{7-\delta}$ 61

5 Remanent Magnetization 71

5.1 Introduction 71

5.2 Results and Analysis 74

5.2.1 Single Crystal 74

5.2.2 Polycrystalline Total Flux 79

6 Conclusion **88**

Nomenclature **91**

Bibliography **94**

List of Figures

1.1 The applied field on SC samples (a) below H_{c1} , (b) in the vortex state 3

1.2 The structure of $YBa_2Cu_3O_7$ 6

1.3 The layered $YBa_2Cu_3O_x$. (a) Cu-O plane, the charge reservoir layer which plays the most important part in oxygen stoichiometry and disorder states, (b) Cu-O planes in the layered $YBa_2Cu_3O_x$ 7

1.4 The variation of T_c vs the oxygen content according to several key-experiments and theoretical calculations. After R. Schleger [56]. . . . 8

1.5 The irreversibility line. After Muller et al. [48]. 13

1.6 The ZFC hysteresis loops for YBaCuO at different temperatures. After Senoussi et al. [57] 15

2.1 The VSM system 19

2.2 The variable temperature cryostat 21

2.3 Helium Transfer Replenishment 22

2.4 The home made quenching station used to quench the SC sample from different temperatures to produce different oxygen contents and disorder states. 26

2.5 The T_c measurement for the as-prepared sample 31

3.1 The microscopic picture of currents inside the SC sample 34

3.2 The Bean's model 36

3.3 Critical current densities deduced from magnetization hysteresis at 4.2K as a function of magnetic field either parallel or perpendicular to Cu-O plane. 39

3.4 The variation of the ratio of $\frac{J_c^c}{J_c^{ab}}$ with magnetic field. 41

3.5 Variations in J_c with magnetic field parallel with Cu-O plane at different temperatures. 41

3.6 The field dependency of J_c for as prepared sample (x=6.8) at different temperatures. 43

3.7 The field dependencies of J_c at different oxygen content a) x=6.41, b) x=6.5 c) x=6.64 46

3.8 The field dependencies of J_c at different oxygen content a) x=6.7, b) x=6.8 c) x=6.9 47

3.9 The J_c at certain applied fields vs the oxygen content. 48

3.10 a) The field dependency of J_c for the disordered state at x=6.5 and b) the variation of the ratio of $\frac{J_c(disorder)}{J_c(order)}$ with the field. 51

4.1 The hysteresis losses of single crystal YBCO at 4.2 K and with field applied parallel to the ab-plane. 57

4.2 Hysteresis losses on single crystal YBCO at 4.2 K and with a field applied parallel to its c-axis. 58

4.3 Energy losses for the as-prepared polycrystalline $YBa_2Cu_3O_x$ with x=6.86. 61

4.4 The field dependencies of energy losses at different oxygen contents of polycrystalline $YBa_2Cu_3O_x$ with (a) x=6.41 (b) x=6.5 and (c) x=6.64 64

4.5 The field dependencies of energy losses at different oxygen contents of polycrystalline $YBa_2Cu_3O_x$ with (a) x=6.7 (b) x=6.8 and (c) x=6.9 65

4.6 Maximum (or saturated) energy losses vs oxygen content in polycrystalline $YBa_2Cu_3O_x$ 67

4.7 The field dependencies of energy losses at oxygen ordered (a) and disordered states (b) of polycrystalline $YBa_2Cu_3O_x$. 70

5.1 The total flux of single crystal YBCO at ZFC state for an applied field parallel and perpendicular to the ab-plane. 75

5.2 The variation of the ratio of $\frac{IRM(c)}{IRM(ab)}$ with the field. 76

5.3 The total flux of single crystal YBCO at FC state for an applied field parallel and perpendicular to the ab-plane. 77

5.4 Total flux for the as-prepared polycrystalline YBaCuOx with x=6.86. 79

5.5 The field dependencies of total flux at different oxygen contents of polycrystalline $YBa_2Cu_3O_x$ where a)x=6.41 b)x=6.5 and c)x=6.64 . . 82

5.6 The field dependencies of total flux at different oxygen contents of polycrystalline $YBa_2Cu_3O_x$ where a)x=6.7 b)x=6.8 and c)x=6.9 . . . 83

5.6b Saturated total flux (at 90 kOe) vs oxygen content for FC and ZFC states 85

5.7 The field dependencies of total flux for the ordered (a) and disordered (b) states of polycrystalline $YBa_2Cu_3O_{6.5}$ 87

List of Tables

1 The dimension of the samples 28

2 Summary of the treatments on the samples and their results 31

3 The initial slopes of energy losses curves 66

Chapter 1

Introduction

Onnes in 1911 discovered one of the superconducting properties in mercury while measuring its resistance with decreasing temperature. He discovered that the resistance dropped to zero below 4.2 K defining a transition or a crititical temperature T_c. The second characterising property is perfect diamagnetism which was discovered by Meissner in 1933. When a superconductor (SC) sample is subjected to an applied magnetic field (at $T<T_c$) the field will be expelled out of the sample interior as long as it is below a critical field (H_c) . The critical field is related to the critical temperature by Tuyn's formula :

$$H_c(T) = H_c(0)\left[1 - \sqrt{\frac{T}{T_c}}\right] \tag{1.1}$$

where $H_c(0)$ is H_c at zero temperature [31].

There are two characteristic geometric length parameters that characterize a superconductor material, namely the coherence length (ξ) and the penetration depth

(λ). The coherence length (ξ) is interpreted as the distance over which the electrons in cooper pair remain together, or as the smallest dimension over which superconductivity can be established or destroyed. The penetration depth (λ) describes the variation of the magnetic field inside the superconductor written as:

$$H(z) = H(0)\exp(\frac{-z}{\lambda}) \tag{1.2}$$

where H and z are the field and the depth from the surface respectively. The values of ξ and λ are in the range of 10 to 10^3 nm.

Superconductors are divided into two types depending on the ratio of these length parameters ($\frac{\lambda}{\xi} = \kappa$) commonly known as the Ginzburg-Landau (GL) parameter [24].

- Type I superconductors have GL parameter (κ) less than $\frac{1}{\sqrt{2}}$. Type I superconductors completely expel the magnetic field from its interior for applied fields less than H_c. Applied fields larger than H_c will completely destroy the superconducting state.

- Type II superconductors have GL parameter (κ) larger than $\frac{1}{\sqrt{2}}$. They completely expel the magnetic field below H_{c1}, and partially expel the magnetic field for applied fields in the range of H_{c1} up to H_{c2}, whereas beyond H_{c2} the superconducting state is destroyed.

After the discovery of superconductivity in mercury samples, many of the elemental metals were discovered to be of type I superconductors, while copper, silver, and gold which are excellent conductors do not exhibit superconductivity down to

very low temperatures (few mK). By the 1950s, some compounds of transitional and actinide series were found to be (conventional) type II superconductors. Their values of T_c and H_{c2} are very large compared with T_c and H_c of type I .

Type II superconductors exhibit an interesting feature when subjected to an applied field in the range H_{c1} to H_{c2}. The field partially penetrates the material in regions, turning them into normal conductors surrounded by superconducting areas. The material is then in a mixed state of superconducting and normal regions commonly known as a vortex state (see fig.1.1). The existence of this state was first predicted by Abrikosov where the magnetic flux penetrates the materials in the form of flux lines, each carrying a single flux quanta (Φ_o). Moreover, the flux lines have a well defined lattice structure. Abrikosov's prediction was verified by the experiments of Essmann's et. al. which showed the triangular flux line lattices [23].

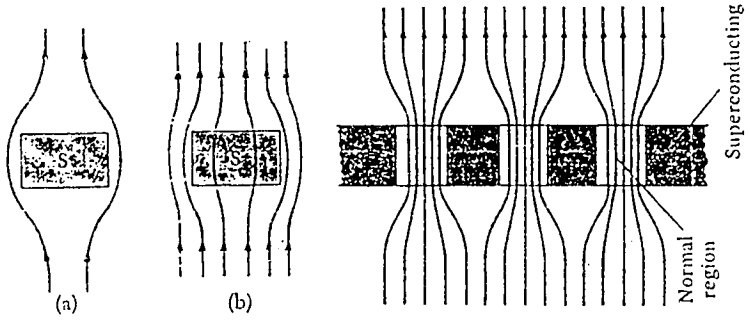

Figure 1.1: The applied field on SC samples (a) below H_{c1} , (b) in the vortex state

The radius of a vortex lines, according to the London model of vortex lines, is ξ. The material is visualized as having normal conducting lines surrounded by the superconducting state. The local field attains its maximum at the vortex centre and vanishes exponentially beyond λ. Clem then extended the London model by proposing the variational parameter (ξ_v) for the vortex radius and introduced the field dependent

penetration depth (λ_{eff}) [23].

1.1 High Temperature Superconductor

Early in 1986, Bednorz and Muller discovered a new type II superconductor. It is a ceramic oxide (Ba-La-Cu-O) that has a perovskite structure with T_c about 36 K and H_{c2} about 36 gauss. This was a great jump in T_c from the highest known conventional superconductor with $T_c \simeq 23.2$ K of Nb_3Ge [31] and marked the beginning of a high T_c superconductivity (HTSC) era which is based on the ceramic oxide. The HTSC are strong type II superconductors, and can be grouped as follows:

- Yttrium based copper oxide ($YBa_2Cu_3O_{7-\delta}$) has a T_c of about 93 K and was chosen to be the focus of our work. It was discovered in 1987. This compound is the most intensely studied since it is the first superconductor which requires only liquid nitrogen, an inexpensive and abundant coolant. It is also easy to prepare and has a very high H_{c2}. Unfortunately its critical current (J_c) at 4.2 K, is lower than that of Nb-compound, a conventional type II superconductor. Moreover these ceramics are brittle and inflexible [58]. These problems reduce its technological applicability [37].

- Bismuth based copper oxide ($Bi_2Sr_{2-x}Ca_{n-1+x}Cu_nO_{2n+4}$) with a T_c of about 110 K was discovered in 1988 [22].

- Thallium based copper oxide ($Tl_mBa_2Ca_{n-1}Cu_nO_{2(n+1)+m}$) with a T_c of about 125 K [31], was also discovered in 1988,

- Mercury based copper oxide ($HgBa_2Ca_{n-1}Cu_nO_{2n+2+\delta}$) with a T_c of about 135 K (for n=3), is the most recently discovered superconductor found in 1993 [55].

1.2 Oxygen Stoichiometry & The Ordering Problem in $YBa_2Cu_3O_x$

1.2.1 The Structure

The structure of $YBa_2Cu_3O_x$ ($YBCO$) is sensitive to its oxygen content. A schematic view of the unit cell is represented in fig.1.2. The structure for x=7 is orthorhombic with lattice parameters a_o, b_o, c_o of 0.382 nm, 0.389 nm, 1.168 nm, respectively. The space group is Pmmm, and the point group is 2/mmm. The structure is a derivative of the cubic perovskite structure ABO_3.

The unit cell contains 3 perovskite cubes with the central anions alternating between Y and Ba. Since there are 3 anions per unit cell in the ideal perovskite structure, corresponding to 9 possible oxygen sites, then the succession of the layers is ...-{CuO_2-BaO- CuO_2-YO -CuO_2- BaO}-CuO_2....so the composition would be $YBa_2Cu_3O_9$ [2].

The missing oxygen atoms in the central plane and in bottom planes of the unit cell each remove one oxygen atom from the formula unit $YBa_2Cu_3O_9$, leaving the succession of layers along the c-directions ...-{CuO-BaO-CuO_2-Y-CuO_2-BaO}-CuO-....which gives the $YBa_2Cu_3O_7$ composition.

The layered $YBa_2Cu_3O_x$ structure consists of 2 CuO_2 (conducting) planes separated by an Yttrium atom, two BaO layers sandwiching the CuO_2 bilayer, and a

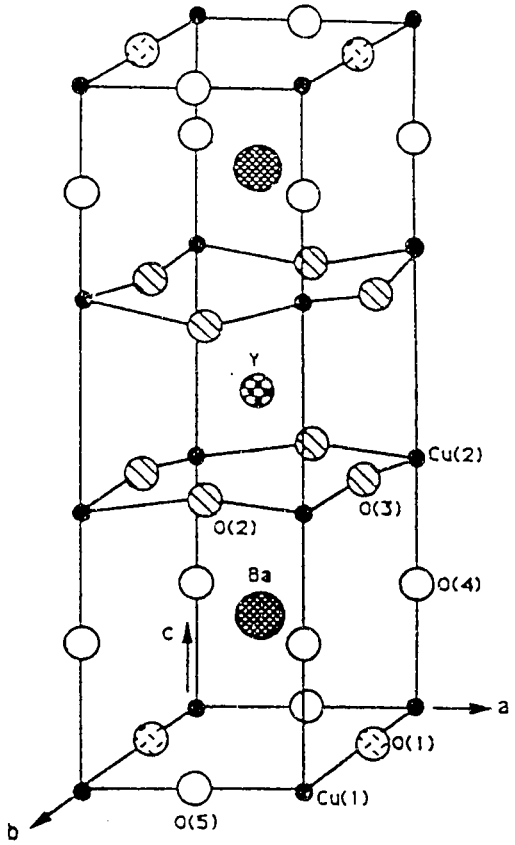

Figure 1.2: The structure of $YBa_2Cu_3O_7$

CuO_x (basal plane) layer (see fig.1.3). The Cu(1), O(1) and O(5) atoms are forming a one dimensional Cu-0-Cu-0-... chain like structure along the b direction known as the "Cu-0 chain" [66].

In a unit cell, there are 2 different types of Cu atoms, namely:

Cu_p or Cu(2) —> Cu in the two CuO_2 planes, and

Cu_c or Cu(1) —> Cu on a four coordinated chain, (p and c referred to plane and chains respectively), while the types of oxygen atoms are :

O(2) and O(3) —>oxygen in the CuO_2 planes, their sites are always occupied

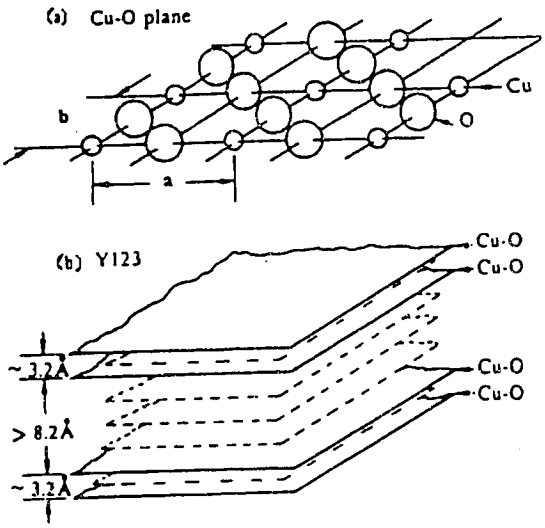

Figure 1.3: The layered $YBa_2Cu_3O_x$. (a) Cu-O plane, the charge reservoir layer which plays the most important part in oxygen stoichiometry and disorder states, (b) Cu-O planes in the layered $YBa_2Cu_3O_x$

O_p or O(4) —>also oxygen in the CuO_2 planes, often referred as the apical oxygen or interstitial site,

O_c or O(1) and O(5) -> oxygen in the chain. (see fig.1.2 for details)

For a comprehensive review of early structural studies of YBCO system, we refer the reader to the review of Beyers and Shaw [4].

1.2.2 Stoichiometry Effects

Oxygen stoichiometry, in $YBa_2Cu_30_x$, is a crucial parameter for controlling structure and superconducting state properties. The oxygen content x can vary from six to seven oxygen atoms per unit cell. At x = 6, both the O(1) and O(5) sites are empty,

the a and b lattice constants are equal and the crystal structure is tetragonal . As x increases, the occupation of oxygen is random with an equal probability to occupy O(1) and O(5) sites due to a strong, direct, nearest neighbour coulomb repulsion [28].

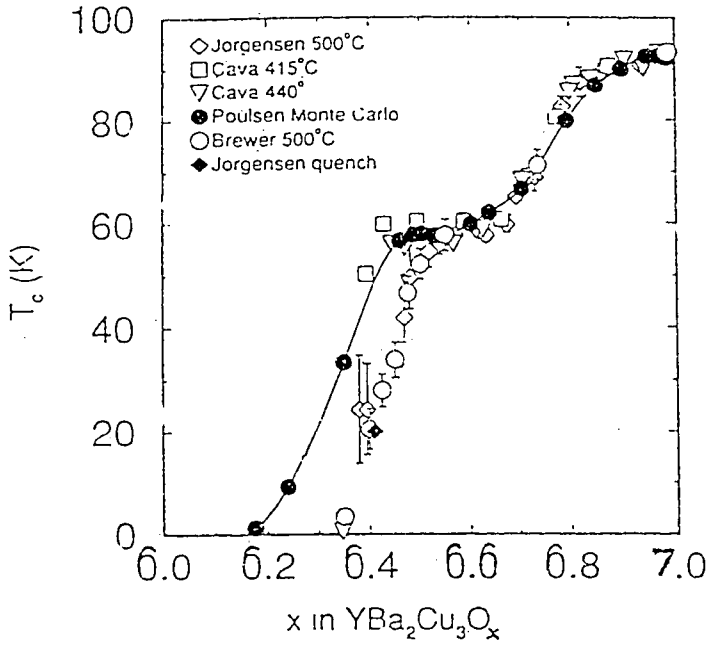

Figure 1.4: The variation of T_c vs the oxygen content according to several key-experiments and theoretical calculations. After R. Schleger [56].

At a critical value (x=6.34), a structural phase transition occurs. Below x=6.34 the structure is tetragonal, and above x=6.34 the structure is orthorhombic with different distortion factors. Oxygen atoms occupy first the O(1) sites while the O(5) sites become empty, this gives rise to the formation of Cu-O chains along the **b**-axis. As a result, the **b**-axis length expands and the **a**-axis contracts, so that the system becomes orthorhombic. Further increases in x results in increased occupancy of the O(1) sites, until at x = 7 all the available O(1) sites are occupied [64][9].

The variation of superconducting transition temperature T_c with oxygen concen-

tration x in the $YBa_2Cu_30_x$ is well established (see figure 1.4)[56]. When x increases in the orthorhombic phase, T_c increases, reaching about 93 K at about x=6.9. The existence of two plateaus at 60 K and 93 K, has been suggested to be due to the existence of two different superconducting and insulating phases [49]. The plateau at 60 K is due to a stagnation of the number of holes doped to the planes as x increases, while the 90 K plateau is due to a saturation effect of T_c [66].

Using the charge transfer (CT) model which suggests that the superconductivity occurs in CuO_2 (conducting) plane [2], we can describe the $T_c(x)$ relation. This description will also be used for the $J_c(x)$, energy losses vs x, and total flux vs x relations in the following chapters.

In the CT model, the number of carriers (holes) in the conducting CuO_2 planes is controlled by the amount of charge transferred from the charge reservoir layer. The charge reservoir is assumed to be the basal plane which provides carriers or a coupling mechanism necessary for superconductivity [49].

In view of the CT model, the O(1) oxygen atom in the basal plane work as a supplier of charge carriers. It attracts electrons from conducting CuO_2 layer and leaves holes there so that when x increases, more oxygens will occupy the O(1) sites in the basal plane. They then attract more electron from CuO_2 layer thus creating higher hole concentration [63]. Correspondingly, it increases the T_c.

1.2.3 Order Disorder Phenomena

It is also found that superconducting and normal properties of $YBa_2Cu_30_x$ not only depend on the oxygen concentration but also on the degree of oxygen order. The term order disorder refers to the positional meaning which arises either when oxygen atoms occupy improper positions or when more positions are available for the oxygen atoms than necessary [28].

Oxygen disorder is usually produced by low temperature annealing of the sample at about 200°C and quenching to room temperature (in alcohol) or to liquid nitrogen temperature . This process is performed after determining the oxygen content. The result is that some of the O(1) atoms will be removed from their sites to occupy the nearby empty sites without any loss of the over all oxygen content. Room temperature aging causes the oxygen atoms to move back to their O(1) sites[1] with mean life time that depends on the oxygen content. The transition temperature is affected accordingly [66].

In view of the CT model, oxygen disordering modifies the density of charge transfer. The supply of charge carriers could only be done by smaller number of the remaining O(1) atoms in the sites. Consequently less electrons can be transferred from the conducting CuO_2 plane. It thus reduces the hole number in this plane and correspondingly it affects (reducing) the T_c.

[1] Room temperature aging has been found to produce changes in T_c as high as 15 K [66].

1.3 Magnetization Measurements

There are two main advantages of using magnetization measurement for SC samples. First, it is a contactless technique which keeps away the heating problem that usually occurs in the current contacts. It is also allows the measurement of very small samples. Second, it is time efficient which reduces problems associated with time dependent properties of SC, such as magnetic time relaxation.

A typical result of magnetization measurements for type II SC is described in fig.1.6. As the applied magnetic field increases, the initial magnetization of the SC sample decreases linearly from zero moment. The slope is about $-\frac{1}{4\pi}$ indicating a zero induction (B) in the interior of the sample (Meissner effect) written as:

$$\begin{aligned} B &= H + 4\pi M = 0 \\ M &= -\frac{1}{4\pi} H \end{aligned} \tag{1.3}$$

Around a lower critical field (H_{c1}), the magnetizations begins to deviate from linearity. As the field further increases, it shows a plateau of minimum values, then turns up increasing slowly and vanishes around an upper critical field (H_{c2}). In between H_{c1} and H_{c2}, the magnetic fluxes penetrate the sample in the form of vortices of normal state. Above H_{c2} the superconductivity of the sample is destroyed.

1.3.1 The Meissner Effect

The Meissner effect (ME) discovered by Meissner & Ochsenfeld in 1933 occurs when an SC spontaneously expels a static magnetic field from its interior. The effect happens

upon cooling the SC sample in an applied magnetic field [24].

To observe a complete ME, the magnetic flux should move freely from the interior of a sample to its surface. Consequently, full flux expulsion is obtained only in materials with a low density of defects that pin the motion of magnetic flux. This condition is obtainable in most elemental SC, unlike what is commonly observed in HTSC [39]. The possible reason for incomplete flux expulsion (Meissner fraction less than unity) is flux pinning. Another reason is that the sample may not be fully superconducting. The latter means that the Meissner fraction measures only the volume-fraction of the superconducting phase. This is perhaps the least interesting from a physical point of view, but important in the intensive search for new and improved high-T_c superconductors.

Experimentally, Krusin-Elbaum et al. discovered that the Meissner fraction is strongly field-dependent in YBCO ceramic and crystalline material, and rises towards 100% at fields usually below 1 Oe [39]. Perez-Ramirez et al. and Malozemoff et al. confirmed a 100% Meissner fractions in their ultra-low field measurements in YBCO ceramics and crystals respectively. While in BiSrCaCuO crystals the Meissner fractions is observed to be around 75% , and in TlBaCaCuO it is also observed to be around 40% [38]. These facts could suggest a way of searching for new SCs since the higher the T_c the lower the Meissner fraction.

1.3.2 The Irreversibility Line

Muller et. al. have first observed the irreversible behavior in LaBaCuO samples subjected to dc magnetization [48]. Using a standard SQUID (Superconducting Quantum

Interference Device) magnetometer they first cooled the sample to low temperature and subsequently applied the field obtaining the "zero-field-cooled" (ZFC) curve labeled I in Fig.1.5. The diamagnetic moment is then measured upon slowly increasing the temperature.

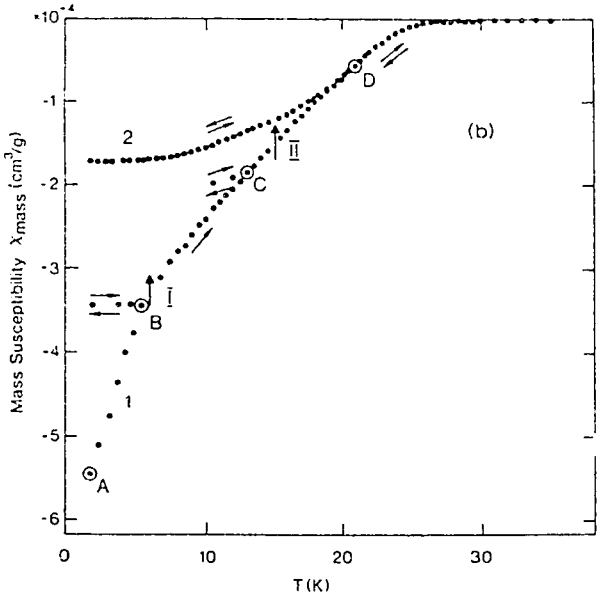

Figure 1.5: The irreversibility line. After Muller et al.[48].

They then slowly reduced the temperature down through its T_c keeping the same field applied during the initial ZFC mode. This state is known as the "field cooled"(FC) Meissner state represented in Fig.1.5 labeled 2. The different magnetization behavior between M_{FC} and M_{ZFC} curves is then referred to as *irreversibility.* Above temperature T*, the M_{FC} and M_{ZFC} curves merged into a common reversible behavior. Moreover they found that this irreversible temperature (T*) is noticeably

lower than T_c and is shifted with field according to

$$1 - \left(\frac{T}{T^*}\right) \propto H^q \tag{1.4}$$

with power q close to 2/3. The curve of T* versus H is then describes as the "irreversibility line".

In classical type II SC, the irreversibility line is due to pinning forces acting on the vortex lines. In HTSC the same characteristics hold, but are easily detected before reaching the $H_{c2}(T)$ line of the H-T phase diagram [48]. Above this boundary, the vortices move quite freely. Muller et al. also discovered that the ZFC magnetization appeared to be unstable and relaxes slowly downward with time. The FC magnetization also discovered appeared to be in equilibrium within experimental accuracy. In YBCO crystals, Malozemoff confirmed that the magnetic relaxation and the irreversibility line has an $H^{2/3}$ dependence [38].

1.3.3 Hysteresis Loops

Hysteresis loop measurements are plots of magnetization versus field. In this plot, the field first increases from zero up to a maximum value, then decreases, reverses in sign, and increases back to the maximum to complete a loop. Many SC features can be understood from this hysteresis loop on the basis of many simple magnetic models such as Bean's critical-state model [5] or its modifications [61]. The critical current density J_c, the critical fields H_{c1} and H_{c2}, energy loss and remanent magnetic moment are commonly treated using Bean's model.

One of the most extensive studies on the hysteresis loops in HTSC has been performed by Senoussi et al. [57].

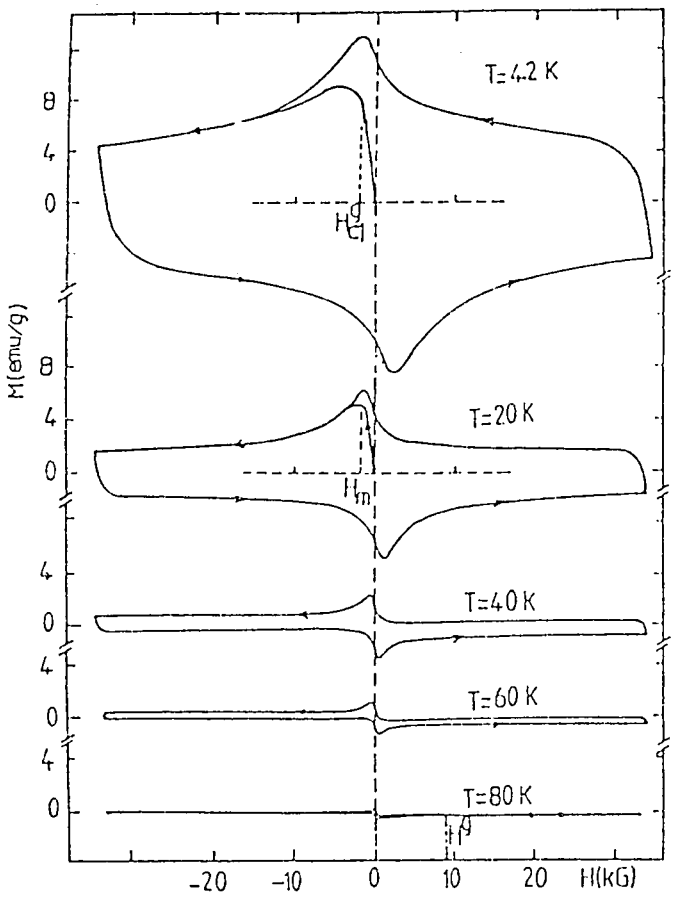

Figure 1.6: The ZFC hysteresis loops for YBaCuO at different temperatures. After Senoussi et.al [57]

The loops in an YBaCuO ceramic are shown in Fig.1.6. The negative magnetization first increases almost linearly with applied field with a slope indicating a high degree of flux exclusion (about $-\frac{1}{4\pi}$). Near a lower critical field H_{c1}, the magnetization begins to deviate away from linearity corresponds to a maximum in the magnitude or a plateau. When the field is lowered from a high value (typically several Tesla), the magnetisation changes sign and usually attains a new plateau that rises to a maximum near zero field.

At higher temperatures the amplitude of the M-H loop shrinks rapidly, and at T^* (irreversible temperature where the sample becomes non-hysteretic), the hysteresis entirely disappears at high fields leaving an almost equilibrium M-H loop.

1.3.4 Field Cooling and Zero Field Cooling

It is important to recognize the basic difference between the zero-field cooled (ZFC) and field-cooled (FC) data. In the FC mode, the field H_{cool} is applied at $T>T_c$. The sample is then cooled down to a measurement temperature $T_m < T_c$. The magnetic field is then reduced to zero and cycled to $\pm H_{cool}$ to produce a full/half hysteresis loop. While for ZFC mode, no field is applied at $T>T_c$. The sample is then cooled down to $T_m(< T_c)$ and the magnetic field is cycled to produce a full/half hysteresis loop.

Since flux is initially absent from the sample during zero-field-cooling, the observed diamagnetism after applying a field represents flux *exclusion* from the sample. In contrast to the zero-field-cooled case, field-cooling starts with flux uniformly present in the sample above T_c . Therefore, any diamagnetic moment M_{FC} which appears as a result of field-cooling represents a flux *expulsion*, often referred as Meissner data [38].

1.4 Motivation

The reason for choosing $YBa_2Cu_3O_z$ in this work is that this material is the most extensively studied SC material. The phase diagram of the oxygen content versus T_c is well established. Besides the abundant experiment and theoretical data on the magnetic properties of $YBa_2Cu_3O_x$, less information is available about the effect of oxygen stoichiometry and disorder on the remanent magnetization and the energy losses. This fact motivated us to carry out this work in order to achieve the following

goals for different oxygen contents of polycrystalline $YBa_2Cu_3O_x$:

- To further understand the energy losses and hysteretic behaviors of this material system.

- To check the applicability of Bean's critical state model in this system by using it to extract the magnetic J_c and its behavior with field and temperature and check its applicability to remanent and magnetic energy losses data.

Chapter 2

Experimental Procedures

2.1 Magnetization Measurement

The magnetic moment measurements were performed using a computer controlled PAR-Lake Shore 4500/150A variable temperature Vibrating Sample Magnetometer(VSM) system. It combines a VSM with a high field superconducting solenoid generating magnetic field up to 9 Tesla, and a variable temperature cryostat in the range of 1.8 to 300 K.

The VSM system consists of the following major parts as shown in Fig.2.1:

1. A vibrating head and sample holder.

2. A variable temperature cryostat.

3. A temperature controller.

4. A VSM controller.

5. A power supply and controller.

6. A PC 486 with a Texas Instrument IEEE-488 GPIB connected to all controllers

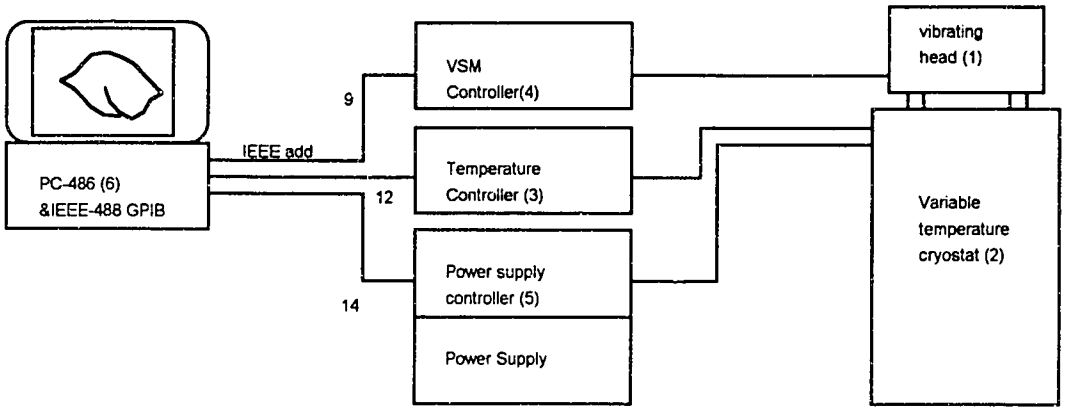

Figure 2.1: The VSM system

2.1.1 Vibrating Head and Sample Holder

A drive head which vibrates the sample rod vertically at 82 Hz is mounted above the cryostat. The vibrating sample is set in motion by a set of capacitor plates. These plates provide a feed back signal to the VSM controller for nulling out components of signal due to vibration not related to magnetic moments. The drive mechanism is composed of a permanent magnet and drive coil such as can be found in an ordinary loudspeaker. The drive assembly is mounted on a damper plate, upon which vibrating damper weights are mounted. These weights vibrate in resonance with the vibration of the sample rod to counteract vibration transmitted through the rigid assembly.

A small sample, whose magnetic moment is to be measured, is mounted at the end of the sample rod suspended inside the core of the superconducting magnet. As the sample vibrates, it produces a changing flux which induces an emf in a pair of stationary pickup coils. The output of the coils is monitored on the digital panel meter of the controller of the vibrating head assembly.

The induced emf in the pick-up coil is dexcribed here according to Faraday law:

$$V = -NA(d\mathbf{B}/dt) \tag{2.1}$$

Integrating this expression gives :

$$\int V dt = -NA(\Delta\mathbf{B}) = -NA(\mu_o\mathbf{M}) \tag{2.2}$$

The signal picked up by the coils is proportional to the magnetic moment **M** of the sample, amplitude, and frequency of vibration. This signal being an a.c. signal of fixed frequency is processed (normalized) to provide a readout of a moment that is proportional only to the moment of the sample. This is done by measuring the difference in magnetic induction between a region of space with and without the sample. The measurement range extends from $5x10^{-6}$ to $1x10^{4}$ emu.

2.1.2 Variable Temperature Cryostat

The cryostat hosts the superconducting magnet, and feeds the sample zone with liquid He at the required temperature. The dewar assembly has a liquid nitrogen reservoir and a liquid helium reservoir, with a vacuum jacket surrounding both reservoirs (see Fig.2.2). The liquid helium reservoir hosts the superconducting magnet and sample cool-down provisions. The vacuum jacket and liquid nitrogen reservoir serve to conserve liquid helium by reducing heat transfer from the environment.

The nitrogen jacket can also be used to pre-cool the superconducting magnet to conserve liquid helium on initial cool-down. After pre-cooling the superconducting

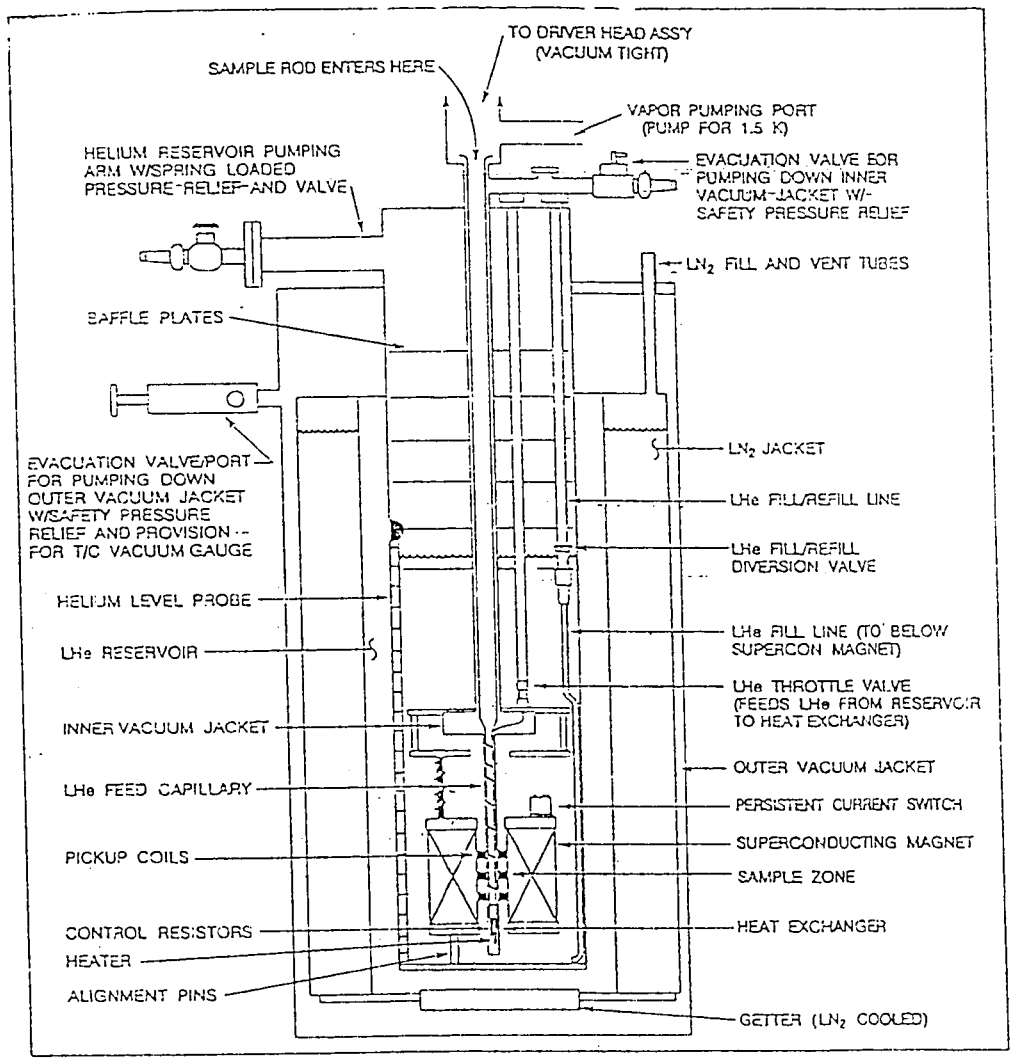

Figure 2.2: The variable temperature cryostat

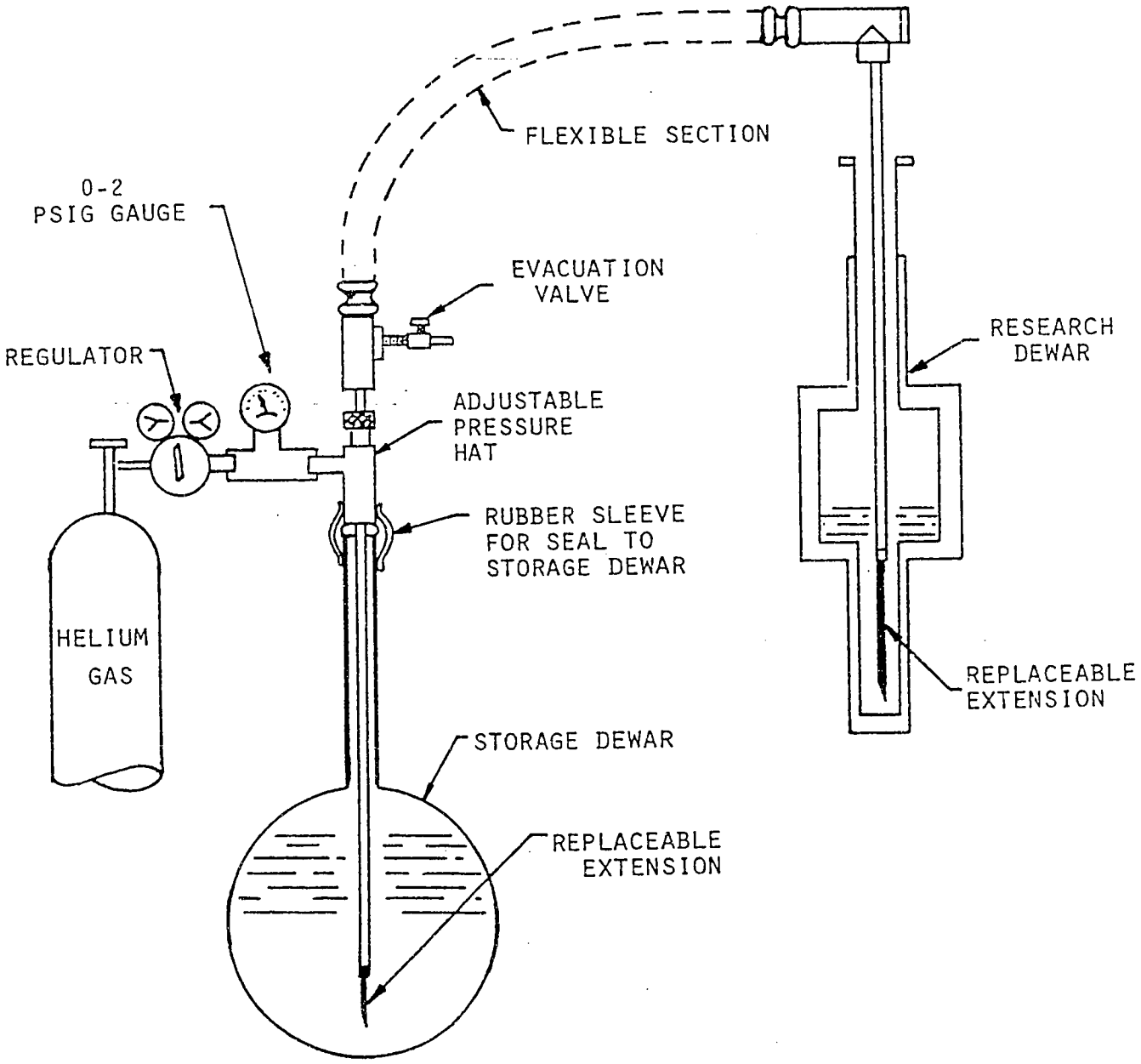

Figure 2.3: Helium Transfer Replenishment

magnet with liquid nitrogen, the inner reservoir is completely emptied of liquid nitrogen by flushing/pumping and re-filling with liquid helium.

A fill/replenish diversion valve is provided that allows the incoming helium to be directed either to the bottom or to the top of the liquid helium reservoir as shown in Fig. 2.3. Each time replenishment is made, some liquid helium will vaporize in cooling the transfer line. If the replenishment were directed to the bottom, this vapor would bubble through the liquid helium in the cryostat,consuming excess liquid helium.

The area surrounding the sample zone, capillary tube, heat exchanger, and sensors is evacuated. This vacuum jacket isolate the temperature sensors from the liquid helium so that they are not influenced by the temperature of the liquid helium reservoir. Another advantage of this inner vacuum jacket is that it reduces the loss of liquid helium by heat transferred from the sample tube.

2.1.3 Temperature Controller

To measure the temperature in the sample zone, field independent carbon glass and platinum resistance thermometers are used. The sample is cooled by helium vapor. Helium is routed from the reservoir through a *throttle valve* and *capillary*. It is then vaporized when passing around the heater in the heat exchanger below the sample. The vapor then passes the sample, cooling or heating the sample to the temperature of the vapor. The helium vapor can cool the sample down to about 2 K if a roughing pump is connected to the sample zone.

Carbon glass and platinum sensors also allow temperature control at the heat exchanger. These temperature sensors are mounted very close to the sample. The

reason being that it is difficult to install the sensors at the vibrating rod, while measuring the magnetic moment.

A Lake Shore model DRC-91CA is used as a temperature controller. The controller main features and specifications are:

- Two sensor input card slots (Carbon glass & platinum), interchangeable and expandable to 6 sensors.
- Precision options which improve sensor display accuracy to between 1 and 100 mK.
- Five digit LED display with selectable resolution and units.
- Setting the control setpoint is achieved via the front panel keypad or through the computer interface.
- The heater power output is a variable DC current source with 25 Ω and 25 watts sources.

2.1.4 Power Supply and its controller

The magnet power supply system consists of two instruments : a mainframe Model 612 and a control unit Model 601 . The system has the following main features:

- Four quadrant outputs with a maximum of ± 125 A and ± 30 V.
- A programmable system for either constant current or constant voltage operation.
- No current reversal switch is required.

- The capacity to source or sink up to 1000 VA continous.
- The standard display and programming resolution is 10 mA and 10 mV.
- Setting and monitoring all operating parameters are achieved via Control Unit front panel keypad/display, computer interfaces, or through the Mainframe analog inputs and outputs.

The power supply controller also hosts:

- A liquid helium level meter connected to the sensor inside the cryostat,
- A gaussmeter connected to a cryogenic Hall sensor located inside the cryostat with the accuracy and reproducibility of approximately 0.5 %.
- Persistent switch heater located at the top of the magnet is a superconducting strip with a heater wrapped around it. The switch works as a shunt, when heated it becomes non-SC and allows the current to pass to the solenoid (controlled mode of operation). If the heater is turned off, the switch then becomes superconducting so that the current is trapped and persistent in the solenoid via the strip; the magnet is then in a persistent mode of operation. In this mode, the coil provides a highly stable magnetic field.

2.1.5 Quenching Station

Quenching Station is described in Fig.2.4 which has been constructed to produce different oxygen stoichiometry and disorder states of the sample. It consists of :

1. Furnace,

2. Valves,

3. Nitrogen, Oxygen, and Argon gas tubes.

4. Quartz tube,

5. Temperature controller

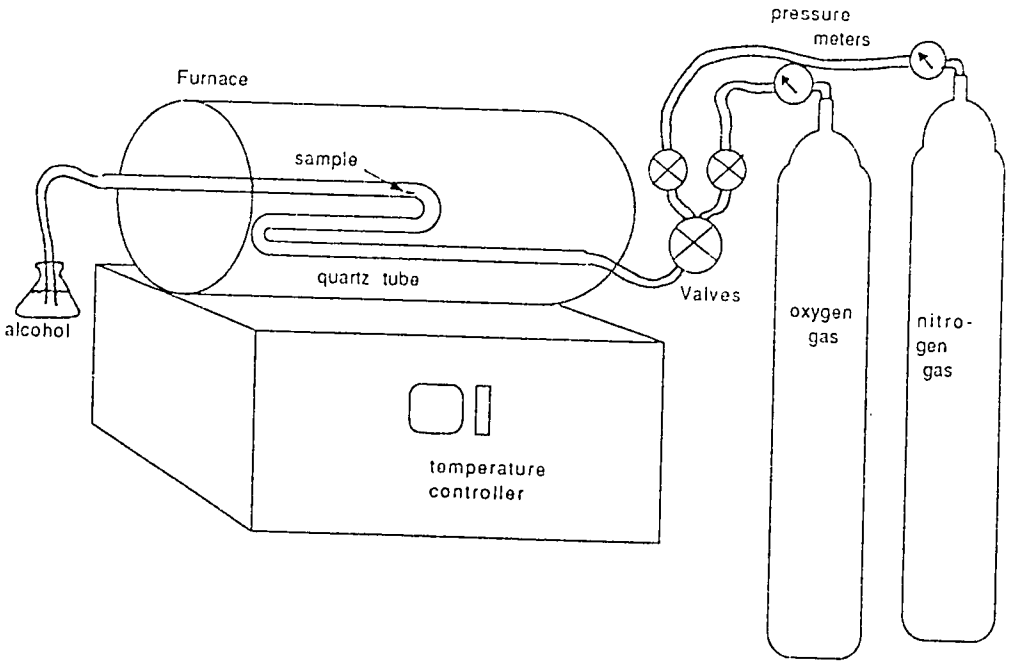

Figure 2.4: The home made quenching station used to quench the SC sample from different temperatures to produce different oxygen contents and disorder states.

The sample is located as described in the above figure. The oxygen stoichiometry is then controlled by annealing the sample at certain temperatures under an O_2 or N_2 atmosphere. For increasing the oxygen content, O_2 is used; while N_2 is used for decreasing the oxygen content. Argon gas, a noble gas which does not react with the samples, is used to quench the sample from 200-600°C to liquid nitrogen or to room temperature.

2.2 Sample Preparation

The samples used in this work are single crystal and polycrystalline $YBa_2Cu_3O_x$. The single crystal sample was prepared at Argonne National Laboratory, Chicago, Illinois, USA., while the polycrystalline samples have been prepared in Superconductor Lab. of Physics Dept. of KFUPM.

There are three common methods on $YBa_2Cu_3O_x$ polycrystalline sample preparation namely : solid state reaction, co-precipitation, and sol-gel techniques [37]. In this work, we used the simplest one that is the solid state reaction technique to produce high quality samples.

Stoichiometric ratios of Y : Ba : Cu = 1:2:3 using high purity (99.999%) powders of Y_2O_3, $BaCO_3$, and CuO were mixed thoroughly. The powders were mixed and ground using an agate mortar and pestle for about half an hour. The mixture was placed in alumina crucible and then calcined in a furnace in air at 800°C for about 8 hours. During the calcination process, carbon is released from $BaCO_3$ as CO_2. After fast cooling to room temperature, the samples are re-ground and the calcination process repeated at 850°C for about 5 hours, 900°C for about 6 hours, and 950°C for about 15 hours. The resultant mixture was re-ground and pressed into 2-3 mm thick, 10-13 mm diameter pellets at a pressure of 4000 kg/cm^2. Finally, pellets are sintered in oxygen gas at a temperature of 900° C in a tube furnace for about 15 hours. The pellets are cooled down slowly (1°C per minute) to 400°C then furnace cooled to room temperature. These annealed pellets were further re-ground, pelletized under the same conditions and the annealing procedure was repeated for at least one more

time. A bar of approximate dimension $2 \times 2 \times 5\ mm^3$ was then cut from the pellet and found to be suitable for sample holder size of the VSM. Three such bars were then taken as prepared samples with the same $T_c = 90K$ and they have the following specifications reported in table 1.

Table 1. The dimension of the samples

Material :	weight (mg)	volume (mm^3)
single crystal	2.2	1.86×1.42×0.45
polycrystalline:		
a	58	5.2×1.8×1.7
b	66.2	4.37×3.32×0.93
c	77	4.6×3.1×2.75

2.2.1 Preparation of Different Oxygen Content and Disorder Samples

The oxygen stoichiometry is controlled by annealing the samples at $T \approx 600°C$ in O_2 gas flowing through the quartz tube of the quenching station. The sample is then quenched using a blast of high pressure Argon gas. Oxygen stoichiometry is readily reproduced in this way with high precision as has been shown in detail by Jorgensen et.al and Cava et.al. [28, 9]. In our case, the stoichiometry state is translated directly from its T_c result using the phase diagram of oxygen content vs T_c [56, 66]. By measuring the magnetization as a function of temperature in the presence of a small magnetic field (75-100 Oe), the SC to normal transition curve is obtained . The T_c is then determined by extrapolating to zero the linear part of the transition curve.

Oxygen contents of 6.8, 6.86, and 6.9 have been obtained using sample a of table 1. The corresponding transition temperatures are shown in table 2. The superconducting properties of the as-prepared sample with x=6.86 was destroyed first by annealing at 900°C in N_2 for about 14 hours. It is then introduced in the quenching station and annealed at 600°C in O_2 for 30 minutes after which it is quenched to room temperature. The T_c of this quenched sample is 88K corresponding to $x = 6.8$. After a complete magnetic measurement in the FC and ZFC modes, the sample was annealed at 600°C in O_2 for 15 more minutes. The total annealing time for this 'a' labelled sample is 45 min. The sample is then quenched to room temperature and the T_c for this 45 min. annealed sample is 93 K corresponding to $x = 6.9$.

A similar heat treatment has been performed for the sample labelled 'b'. First, superconductivity of the sample was destroyed by annealing at 900°C in N_2 for about 41 hours. This is then followed by annealing at 600°C in O_2 for 3 minutes and quenching to liquid nitrogen temperature. The T_c of the quenched sample is 32K corresponding to $x = 6.41$. After a complete magnetic measurement was done, the sample was then annealed at 600°C for 2 more minutes completing a 5 min. total annealing time. The T_c for this 5 min. annealed sample is 68.5 K corresponding to $x = 6.64$. A two more min. annealing and quench as described above for this 'b' sample produces a transition temperature close to 90 K. To reduce the transition temperature to the 70-80K range, the sample was annealed in N_2 at 600°C for 2 min. This will reduce the oxygen content of the sample, bring the T_c for this sample down to 72 K corresponding to $x = 6.7$ which is in the required range.

For achieving x=6.5 state, several annealing and quenching processes as described above have been done on 'b' and 'c' samples. However, the results were less satisfactory. Annealing in N_2 was necessary to reduce the oxygen content if it is too high or even to destroyed the superconducting properties of the samples. After some trials, a T_c of 49 K (x=6.5) later was obtained in sample c. This result was obtained from a 1.5 min. anneal in O_2 at 600°C after a long anneal in N_2 at 600°C. The x=6.5 state is interesting in a sense that it has been found to produce a maximum degree of disorder after annealing at 200°C for about 10 min. [66]. A summary of the heat treatments on the samples and their results is presented in table 2. While the plots of magnetization vs temperature for the T_c measurement are represented in Fig. 2.5

Table 2. Summary of the treatments on the samples and their results.

sample:	annealing time (min)	quenched to	oxygen content	T_c(K)
a	45 in O_2	alcohol	6.9	93
a	(as prepared sample)	-	6.86	90
a	30 in O_2	alcohol	6.8	88
b	7 in O_2 + 2 in N_2	LN_2	6.7	72
b	5 in O_2	LN_2	6.64	68.5
c	1.5 in O_2	LN_2	6.5	49
c	20* in air	LN_2	6.5(disordered)	37
b	3 in O_2	LN_2	6.41	32

*= secondary annealing from x=6.5 state at temp.=200oC.

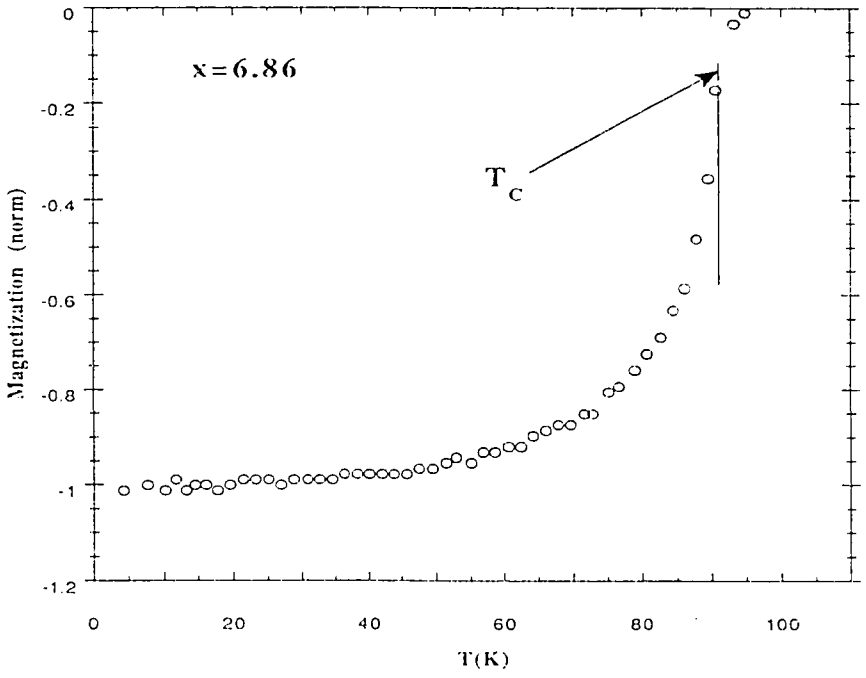

Figure 2.5: The T_c measurement for the as-prepared sample

2.3 Basic Experimental Algorithm

For a given oxygen content and disorder states, magnetic measurements were done on the following magnetic states :

- Zero field cooling (ZFC) state where the sample is cooled through its T_c to the measuring temperature in zero applied magnetic field.
- Field cooled (FC) state where the sample is cooled in fixed magnetic field from above its T_c to the measuring temperature.

While the type of magnetic measurements are :

1. Remanent moment measurement
2. Full hysteresis loops measurements obtained by cycling in different applied fields upto $\pm$ 9 Tesla.

Chapter 3

Critical Current Density

3.1 Introduction

Although T_c sets an upper temperature limit for the possible use of a superconductor, it is the value of the critical current density (J_c) that determines its practical application. For a practical engineering application, it is desirable that J_c be in the range of 10^4 -10^7 A/cm^2 [18] which is now become a target for many SC experimentalists to be achieved.

For any SC material, when the current density exceeded its critical value: J_c, the material transforms to a resistive state. In type I SC the material becomes resistive when the sum of the applied field and the self field induced by transport current exceeds the thermodynamical critical field. In type II, J_c is determined by the strength of the flux line pinning [18].

HTSCs are type II SC and can carry high critical current densities. They contain large amount of defects or impurities that serve as pinning centers for trapping the flux lines. In general, there are many parameters affecting J_c such as temperature, applied field, angle between the applied field, grain size, defects, and impurities. In

the case of YBCO, the anisotropy of the layered structure, or the atomic disorder will also affect the J_c because of its small coherence length ξ (few Å) [37].

To determine the J_c, there are three types of experimental techniques; namely transport or (I-V) characteristics, magnetization measurement (hysteresis loops), and the AC - susceptibility (through its imaginary part of χ)[57]. The J_c obtained from magnetization measurements were found to be larger than the corresponding values obtained from (I-V) characteristics [37]. This problem is usually related to the granularity of HTSC and has been extensively reviewed by Senoussi and can be summarized as follows [57]:

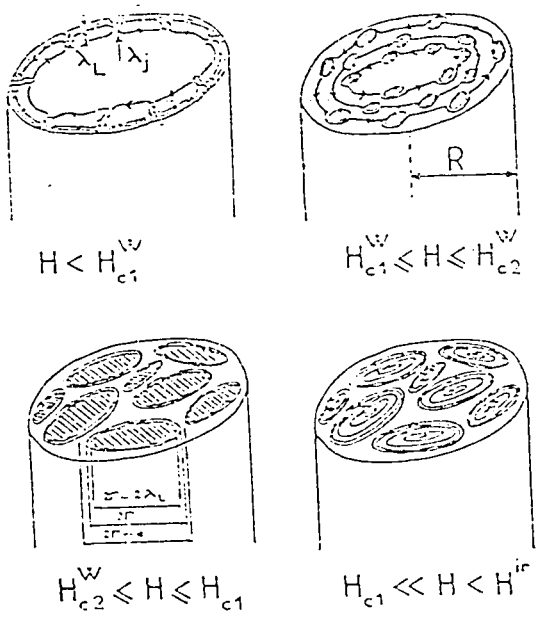

Figure 3.1: The microscopic picture of currents inside the SC sample

- For applied field $H_{app} < H_{c1}^{w}$, the critical field of the weak links, the currents and fields are restricted to the Josephson penetration depth λ_j in the junction between the grains and λ_L in the grains (see Fig.3.1).

- As H_{app} is further increased above H_{c1}^{w}, flux lines penetrate the sample via the weakest links. This gives rise to **inter**-granular current loops (extending over the whole sample) as well as to **intra**-granular current loops around the individual grains.

- At $H_{app} > H_{c2}^{w}$, the inter-granular current vanishes. The magnetic behavior is then due to London (intra-granular) currents surrounding the decoupled grains $(H_{app} > H_{c1})$ [2] .

- Finally at field just above H_{c1}^{grain} vortex lines and the associated intra-granular currents propagate into the interior of the grains.

- Above the depinning line (H_{irr}) the current is restricted to the London-Abrikosov surface currents and becomes zero only above H_{c2}.

The magnetization method which is employed in this work, is an indirect way to determine the J_c. The determination is usually associated with Bean's critical state model. The basic idea of Bean's model for a homogeneous defected type II SC, is described as follows [5, 62]. The model assumes that the J_c is independent of magnetic field i.e.

$$J_c(H) = J_c(0) \tag{3.1}$$

where $J_c(0)$ is the critical current density at zero applied field. The hysteretic mag-

[2] – $H_{c1}^{w} < H_{c2}^{w} < H_{c1} < H_{c1}^{grain}$

netization is related to J_c through a modified Ampere's law

$$\nabla \times h = \frac{4\pi}{c} J_c \tag{3.2}$$

where h is the local magnetic induction inside the superconductor. Bean pictured the penetration of flux from both sides of the sample in terms of a flux gradient. A slab of thickness D is taken with external field H parallel to the slab plane. The boundary condition is h=H_{ext} at the surfaces of the sample (see Fig.3.2)

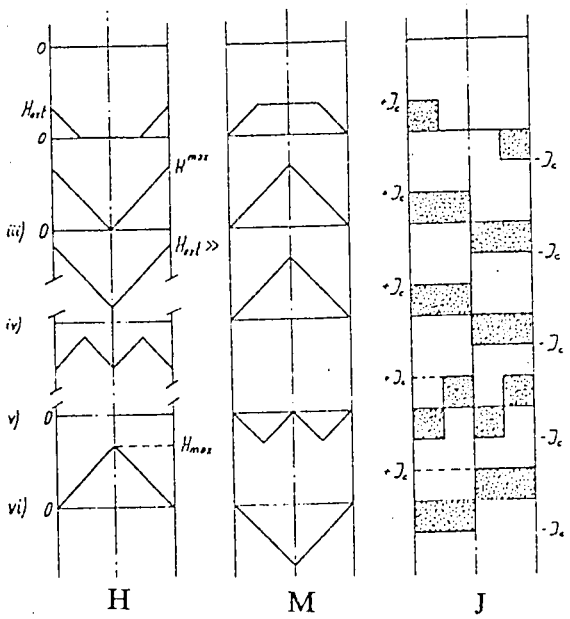

Figure 3.2: The Bean's model

As the field is increased, the flux fronts penetrate further into the sample. At an applied field $H^* = 2\pi DJ_c/c$ the fronts meet at the center of the sample. The magnetization is then the difference of the applied field H and the average flux density (B= H+$4\pi M$) B = $D^{-1} \int dx\ h(x)$ in a slab of thickness D, i.e.

$$4\pi M = \left(\frac{cH^2}{4\pi J_c D}\right) - H, \qquad H < H^* \tag{3.3}$$

For $H > H^*$ and assuming that J_c is independent of field, M will be constant at $M^+ = -J_cD/4c$. The field is then reversed and once the field has been reduced by $2H^*$, a constant M^- is again achieved with the same magnitude as before but with opposite sign. This leads to the "**magnetically determined J_c**" for a SC slab of thickness D with field applied in the slab plane in practical units (A/cm^2, Gauss, and cm)

$$J_c = 30\frac{|-M^+ + M^-|}{D} \tag{3.4}$$

The typical result for polycrystalline HTSC is that the J_c decreases rapidly at low fields then varies with a smaller slope [3] . The weakness of this method is that it does not extract the J_c values above the irreversible line. This is simply because the SC becomes non hysteretic and consequently gives a zero result. However, up until now many scientists are still using the Bean's model. Atzmony et.al. [1] and Grover et.al.[21] have also used Bean's model to describe the observed high field hysteresis loops on HTSC. Instead of considering D as the total sample size, they used it as the grain size.

In our investigations of single and polycrystalline YBCO, the J_c values are deduced from hysteresis loops using Bean's model as depicted in eqn.3.4. In the following sections, we present our results for such a measurement

3.2 Results and Analysis

The J_c dependencies on field and temperature vary slightly from sample to sample. However, some common features are cited here for YBCO samples. The temperature

[3] If J_c has a field dependence, then this formula is best applied at a sufficiently large field to insure a relatively small variation in flux density across the sample.

dependency of J_c shows a rapid decrease with increasing temperature [57]. Moreover, J_c values in single crystal are much less than for polycrystals. The field dependency of J_c, as suggested by Senoussi et.al. together with Groever et.al.[57, 21], exhibits an exponential form. Other suggested forms such as $\frac{1}{B+Bo}$ or $\frac{1}{\sqrt{B}}$ or more general B^{-x} behaviors have also been considered [1, 30].

Dinger et.al. has also observed a large anisotropy in the field dependency of J_c. Here the value obtained along the c-axis (J_c^c) of YBCO crystal is about an order of magnitude larger than J_c in the ab-plane (J_c^{ab}) [17]. The anisotropic ratio ($\frac{J_c^c}{J_c^{ab}}$) ranges from 15 to 25 [15].

3.2.1 Single Crystal Critical Current Density

The variations of the critical current density for the single crystal sample (YBCO) are presented in figs.3.3 and 3.5. Two types of measurements, as mentioned in chapter 1, are customarily used to introduce the field. We have used only the ZFC method to obtain the hysteresis loops at different temperatures and field applied along the ab-plane or along the c-direction of the sample. The obtained J_c values are calculated using Bean's model as described in eqn.3.4 with D (H$\perp$D) taken as the sample size.

Fig.3.3 shows the critical current densities parallel and perpendicular to the Cu-O plane at 4.2 K. A relatively weak decrease with increasing field up to 6T has been seen on both curves. J_c^c ($H_{\|c}$) initially decreases with field then remains almost constant maintaining a relatively high value of $3x10^4 A/cm^2$ up to 6T . It then drops rapidly in a field range from 6 to 9T. The decreasing curves are concave down and exhibits a $\sqrt{H - H_o}$ form with H_o at about 10T . This result is unlike the previously discussed

forms, however it qualitatively agrees with data in the literature at higher field (the concave down behavior). For J_c^{ab} ($H_{\|ab}$), the curve decreases slowly with field (almost constant) maintaining a value of about $4x10^3 A/cm^2$ up to near 9T . Both figures (3.3 and 3.5) illustrate the motion of the flux lines that face a higher degree of pinning in the $H_{\|c}$ direction. This pinning gives rise to irreversible magnetization of the sample and consequently maintains the high J_c values. At higher field, the pinning becomes weaker and exhibits almost the same value in both field directions at 9 T.

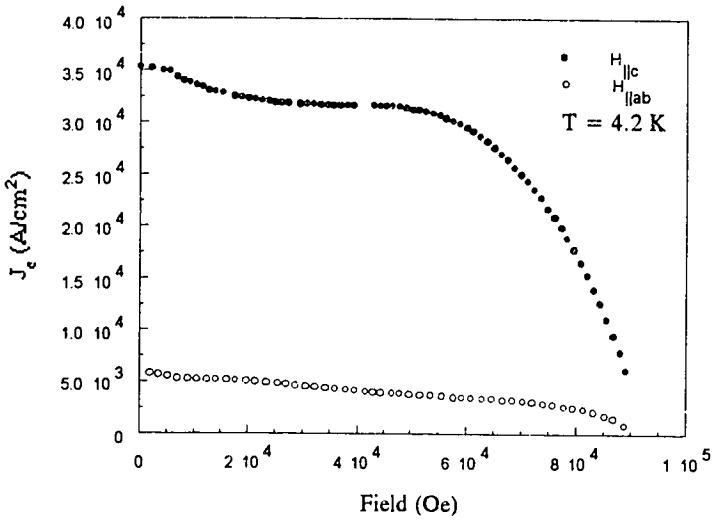

Figure 3.3: Critical current densities deduced from magnetization hysteresis at 4.2K as a function of magnetic field either parallel or perpendicular to Cu-O plane.

It is also observed that initially, up to 6T, the J_c^c is greater than J_c^{ab} by about an order of magnitude reflecting stronger pinning forces in the c-direction than in the ab-plane. The anisotropic ratio ($\frac{J_c^c}{J_c^{ab}}$) then decreases slowly with increasing field up to 6T then decreases rapidly to about a factor of 3 at 9T. These changes are shown

in Fig.3.4. The above result qualitatively agrees with Dinger et.al. However, they couldn't notice the rapid drops at 6T since their experiments were only performed up to 4T.

There are a number of factors that may provide an explanation of the large J_c^c values obtained. First, the difference in spacing of grain boundaries where the supercurrents must face boundaries (that act as pinning centers) more frequently when flowing along the c-axis. Second, a planar defect presumably occurred in the c-axis direction (<001> surface), which is thought to be an excessive Cu-O layer creating a non SC interlayer. Oppositely, a factor that could decrease the anisotropic ratio is the occurrence of twin planes along the ab-plane of our sample, which act as effective pinning centers for the J_c^{ab} [52]. The above result illustrates that YBCO is strongly anisotropic and the induced J_c is higher when flowing perpendicular to the Cu-O planes.

Fig.3.5 illustrates the field dependency of J_c^{ab} at various temperatures. The field is applied parallel to ab-plane which means that there is a pinning contribution from the twin boundaries. The curves at the lower temperatures (2 and 4.2K) shows similar behavior. Initially, both decrease almost linearly with increasing field. Above 7.5T, they drop abruptly with concave down behavior. A plateau in the range of 20-25 kOe is observed at the curve of 2K. The plateau shifted down to the range of 10-15 kOe at 4.2K and reaches the 0-5 kOe range at 40K. A secondary plateau also observed on the same curve at the field range of 55-60 kOe.

At higher temperatures such as 20 and 40 K, the J_c^{ab} curves are observed to be almost linearly decreasing with field except for the initial part at lower fields. The

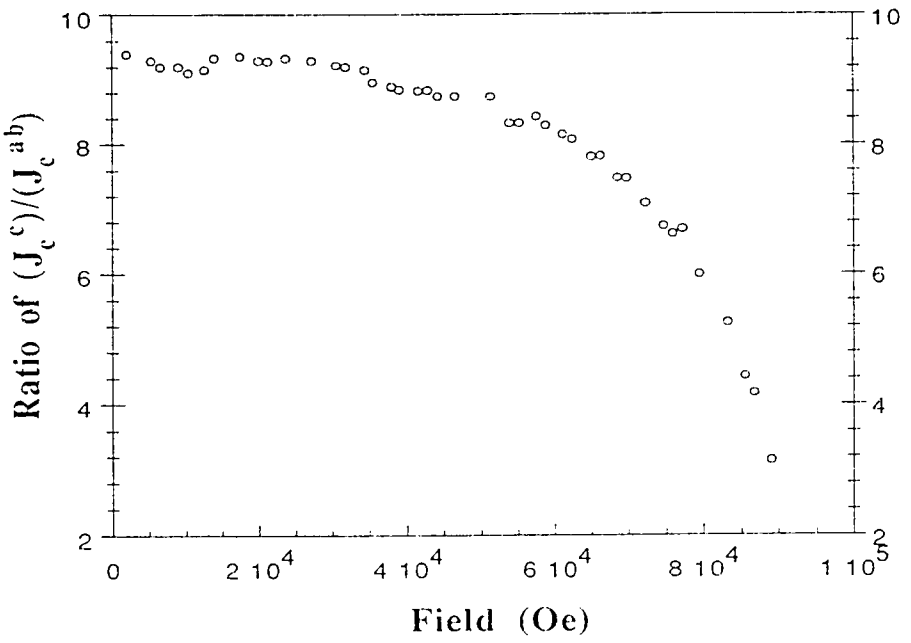

Figure 3.4: The variation of the ratio of $\frac{J_c^c}{J_c^{ab}}$ with magnetic field.

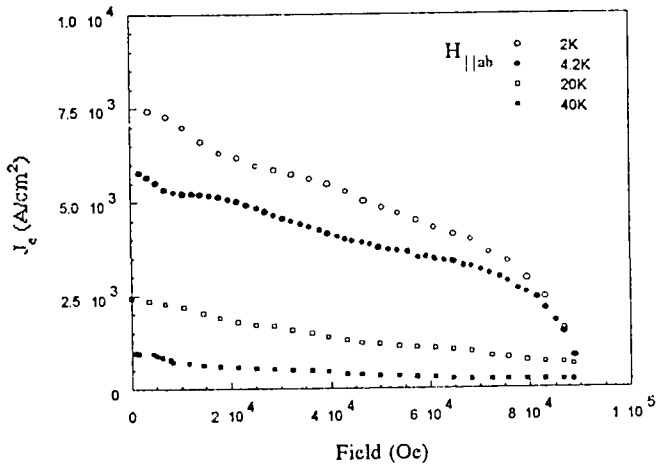

Figure 3.5: Variations in J_c with magnetic field parallel with Cu-O plane at different temperatures.

slopes are smaller compared to those at lower temperatures. Such a linear behavior is consistent with what was observed by Senoussi et.al. [57]. Similar results have also been reported by other groups [?, 15]. At 20 and 40K, J_c^{ab} is reduced to almost zero at 45 kOe respectively. It should also be noted that the lower temperature J_c^{ab} (at 2 and 4.2K) tends to zero at the field somewhere between 90 to 95 kOe. However, at higher temperatures, J_c tends to zero at much higher fields. It seems that the rapid drop in J_c at low temperature may be an artificial result that arises from reducing the field from its maximum value. This temperature dependency can also be understood according to the flux creep phenomenon proposed by Anderson [3].

3.2.2 Polycrystalline Critical Current Density

In our J_c investigation of polycrystalline YBCO, the magnetic measurements were performed up to 90 kOe for the ZFC state only. The results from as-prepared polycrystalline samples are presented in Fig.3.6. J_c values are calculated using Bean's model as described in eqn.3.4 with D taken as the average grain size.

The results in Fig.3.6 showed an exponential decay of J_c, consistent with the previous results reported by Senoussi [57]. Initially, the low temperature curves (2 K and 4.2K) show a mild maxima around zero field, then J_c decreases rapidly up to about 20 kOe. Above that, J_c stays in the range of 10^6 A/cm^2. Finally, near 90 kOe, J_c seems to drop. This drop is not very clear at high temperatures and therefore needs more detailed investigation.

The initial rapid decrease of the curve is a consequence of the low field peak observed in the hysteresis loop. Such a peak is a common characteristic of the granular

nature of polycrystalline HTSC as discussed in the beginning of this chapter. The sharp drop signals the absence of inter-grain currents. It is then followed by a slower drop extending above 20 kOe which may indicate full penetration of intra-grain currents into the interior of the grains.

At higher temperatures (20 to 60 K), the J_c curves were observed to have a similar exponential decay. An interesting feature observed here is that the full penetration field is shifted down as the temperature increases. For example, at 20K, the penetration is about 10 kOe (half of the value at 4.2 K). This shift is a reflection of the temperature dependency of the critical field (H_{c1}) described by Tuyn in conventional SC. A more detailed study of this shift could be a test of the applicability of Tuyn's formula (eqn. 1.1) for HTSC samples.

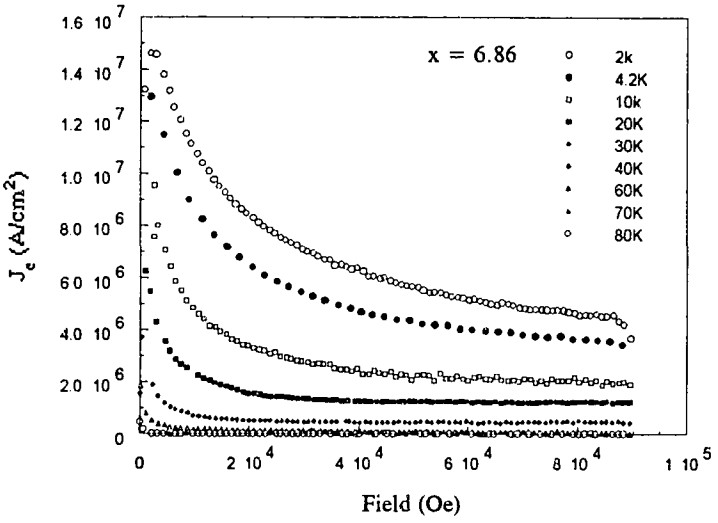

Figure 3.6: The field dependency of J_c for as prepared sample (x=6.8) at different temperatures.

In comparison with the single crystal results, the critical current density of the polycrystalline sample studied, is observed to be greater than that of single crystal by about two order of magnitude. This fact reflects the size dependence of J_c as predicted by Bean's model. The critical current density of the single crystal exhibits a concave down behavior with increasing field over a wide range of field (0-9T), unlike the behavior observed in polycrystals. The initial J_c curves of polycrystalline samples observed to decrease rapidly which is absent in the single crystal (almost exponential decrease). The above differences suggest that the granularity of the polycrystalline samples plays an important role in the J_c behavior. As an additional note, our high field polycrystalline results can only be expressed in terms of the intra-grain behavior of the currents, because the inter-grain currents behavior can be seen in the range of a few hundreds of Oersted.

Oxygen Stoichiometric Effect

The following figures (3.7 and 3.8) illustrate the field dependency of J_c for different oxygen contents in YBCO polycrystalline samples. Generally, the curves in these figures can be divided into 2 regions. The first region shows an exponential decay behavior as suggested by Senoussi et.al. and the second one is a linear decay. The regional changes occur at a transition field which is shifted to lower field as the temperature increases. The high field slopes in the second region are small enough to maintain the J_c values in the order of 10^6 A/cm^2. It is observed that these slopes become smaller for samples with $x \geq 6.64$, as the temperature increases. The opposite behavior is found for $x < 6.64$. This feature can be interpreted (at higher fields)

according to the theory that the oxygen deficient samples are driven faster into their normal state. Moreover, they have lower H_{c2} and T_c than the oxygen rich samples. So that, a rapid decrease in J_c (with higher slopes) in the second region of the curves is expected. This also indicates a weakening in the pinning force as oxygen is being removed, especially from the O(1) sites. Another reason comes from the reduction in the density of carriers in the CuO_2 planes supplied by fewer remaining O(1).

In order to get a complete idea about the effect of oxygen content (x), a plot of J_c(x) was taken on 2, 20, and 40 kOe and presented in Fig.3.9. The choice of fields representing the regional behavior of J_c i.e. 2, 20, and 40 kOe are in the first, second, and the transitional region, respectively. It is observed that J_c increases gradually with increasing oxygen content with the exception of x=6.86. The heat treatment of this state is different than the other states. It was furnaced cooled in flowing O_2 while the other states have been quenched from 600° C to room or LN_2 temperatures. The slope for applied field of 2 kOe is greater than that for 20 and 40 kOe which appear to be parallel. These slopes are not so big giving rise to an interpretation that the chain site oxygen O(1) does transfer the charge-carrier to the Cu-O planes but with a gradual and steady increase.

The deviation from linearity observed at x=6.86 might be related to the work of Daeumling et.al. They ascribed that a small oxygen deficiency (from fully oxidized: x=7) might increase the pinning in single crystals [16]. This remarkable result created a discussion of the role of oxygen vacancies (by removing O(1) from its site) as an effective pinning center.

The transport studies of Wisniewski et.al.[65] on bulk samples and the magnetic

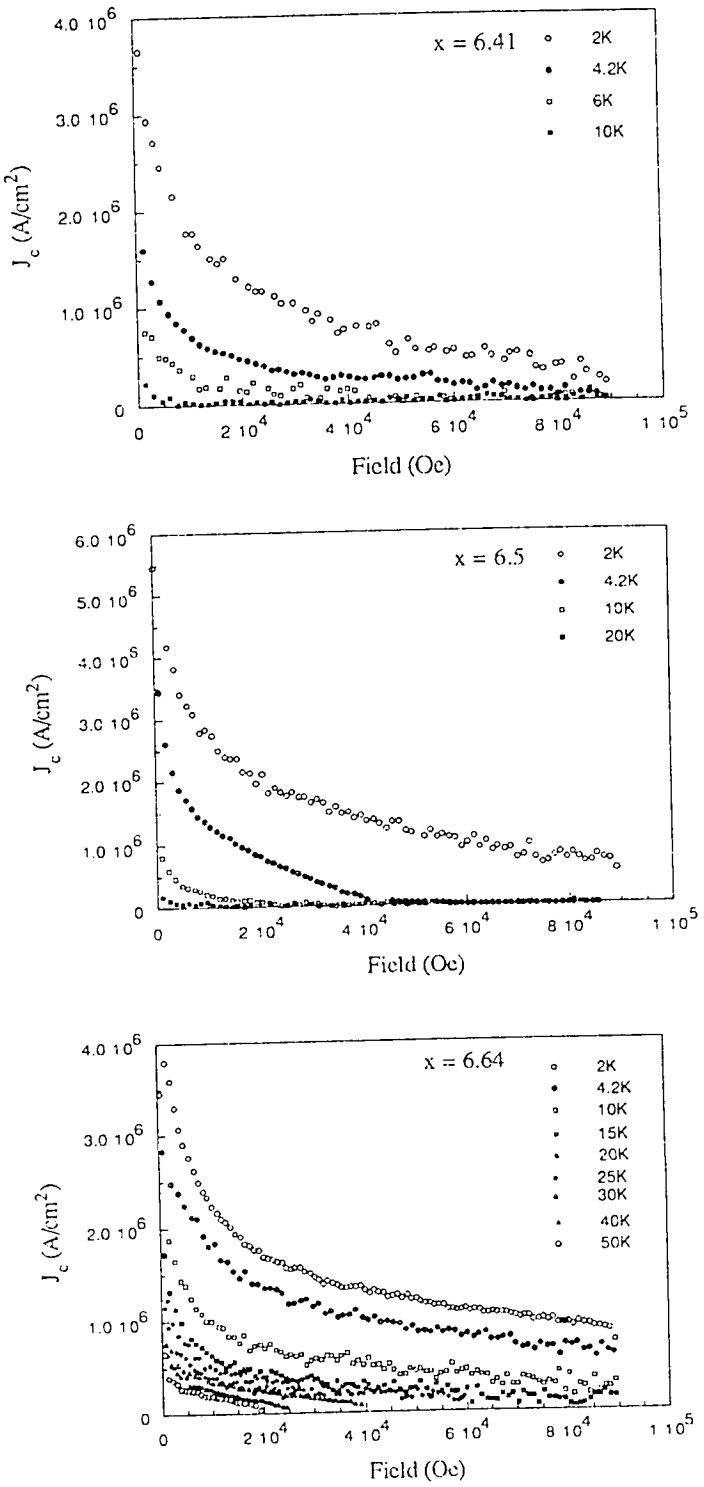

Figure 3.6: The field dependencies of J_c at different oxygen content a) x=6.41, b) x=6.5 c) x=6.64

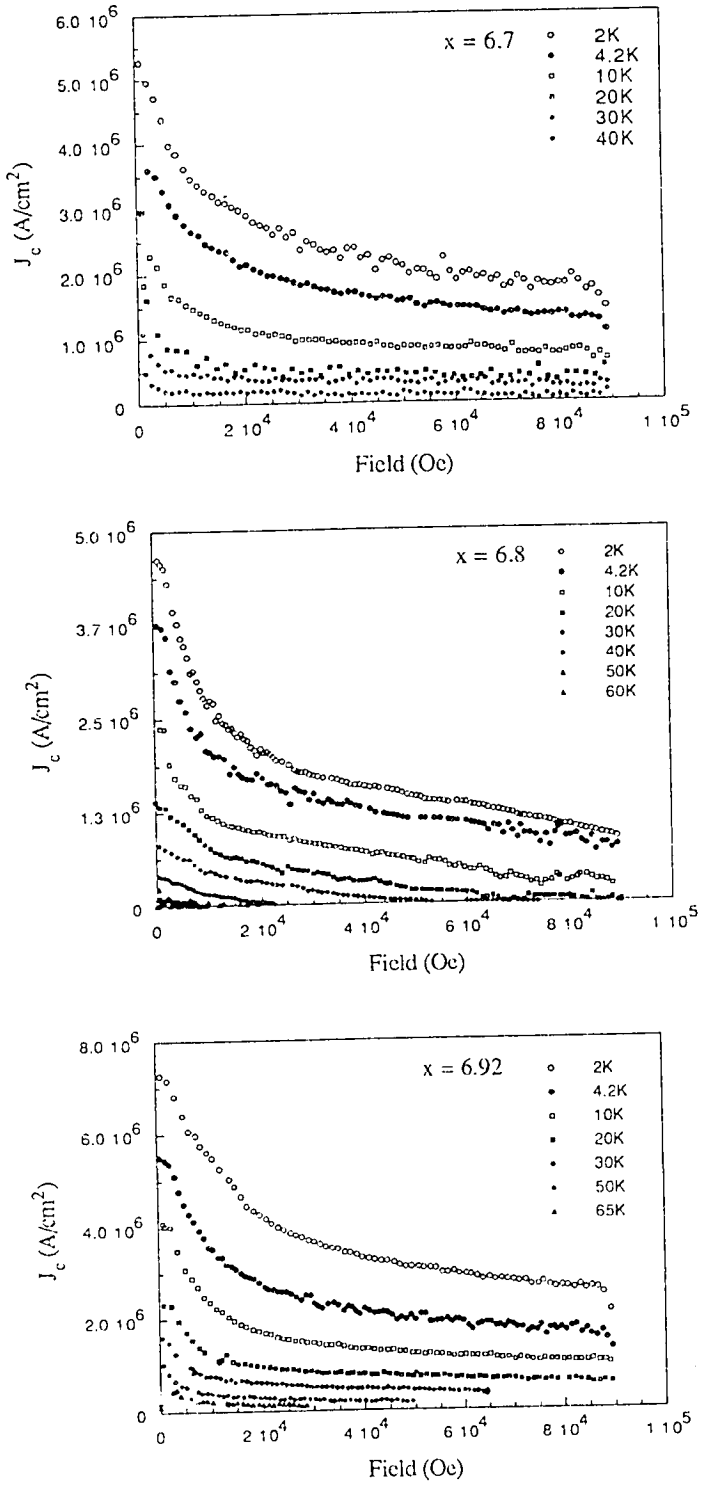

Figure 3.7: The field dependencies of J_c at different oxygen content a) x=6.7, b) x=6.8 c) x=6.9

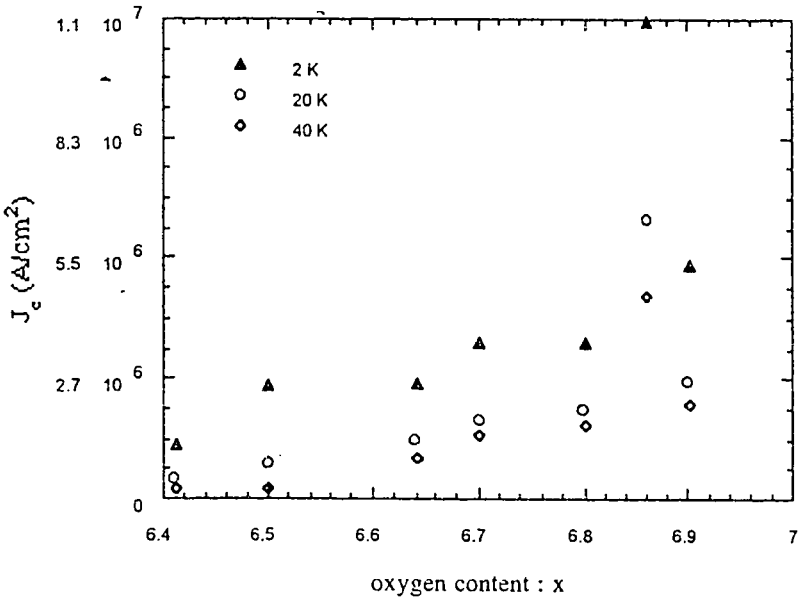

Figure 3.9: The J_c at certain applied fields vs the oxygen content.

measurements of Ossandon et.al. and Christen et.al. [51, 10], they were able to show that $J_c(x)$ exhibits a linear behavior ($x \geq 6.7$). In fact, their results seems to be in agreement with ours. However, they did not report the effect of heat treatment and couldn't find any pronounced deviation from linearity as we have. They then concluded that the chain-site oxygen vacancies are not strong pinning centers, but the strength of effective pre-existing pinning barriers is degraded with oxygen deficiency.

Based on the above results, we proposed that the combined effects of chain site oxygen vacancies, as additional pinning center and the opposite effect of a carrier density reduction at the range of $x \approx 6.86$ play an important role in determining the critical current density in oxygen deficient samples. A more detailed study of oxygen vacancies and carrier density in that range could clarify the above assumption.

Another explanation could be related to the the coherence length ξ studies on different oxygen content done by Vandervoort [63]. As the oxygen content increases, the

coherence length ξ decrease. The decreasing ξ indicates an increased carrier density due to more hole doping from more oxygen atoms in the chains and consequently the superconductivity mechanism is enhanced.

It is also noted that no plateau was found for $J_c(x)$ as has been seen in $T_c(x)$. This indicates that the stagnation of the number of holes doped to the planes at x=6.6 doesn't affect the linear increase of J_c.

Oxygen Disorder Effect

Although the above analysis on stoichiometric effects gives us a general picture of the role of O(1) on J_c, a further investigation on the disorder effect, however seems warranted. For this purpose, a disorder state was created at the oxygen content $x = 6.5$ where a maximum disorder could be obtained. At this x-value, an alternating O(1)-filled and unfilled sites on the b-axis is exhibited. These results are presented in Fig.3.10(a).

It is observed that, initially, the J_c exhibits a maximum around zero field then decreases gradually up to 7 KOe. This is unlike the exponential region observed in the more ordered x=6.5 state. This initial behavior is shifted to lower field as the temperature increases. The J_c value is reduced to half of its value in its ordered state in the exponentially decreasing region. The smaller number of O(1) atoms in the disordered state may modify the distribution of pinning forces thus affecting the charge transfer mechanism. The proposed concept that the O(1) vacancies can act as additional pinning centers is not sufficient to explain this phenomena [19, 50].

The absence of inter-grain currents that give rise to the sharp drop is not clearly seen at 2K, but more pronounced at 4.2K. The deflection/transitional points shifted to lower fields indicates that the field of full penetration of the currents into the grains is lower in the disordered state.

An interesting feature is reflected in the linear region in which J_c has almost the same value as that for the ordered state. A detailed comparison between the ordered and disordered states of J_c is describes by the ratio $\frac{Jc(disorder)}{Jc(order)}$, as a function of field

and these results are presented in Fig.3.10(b)

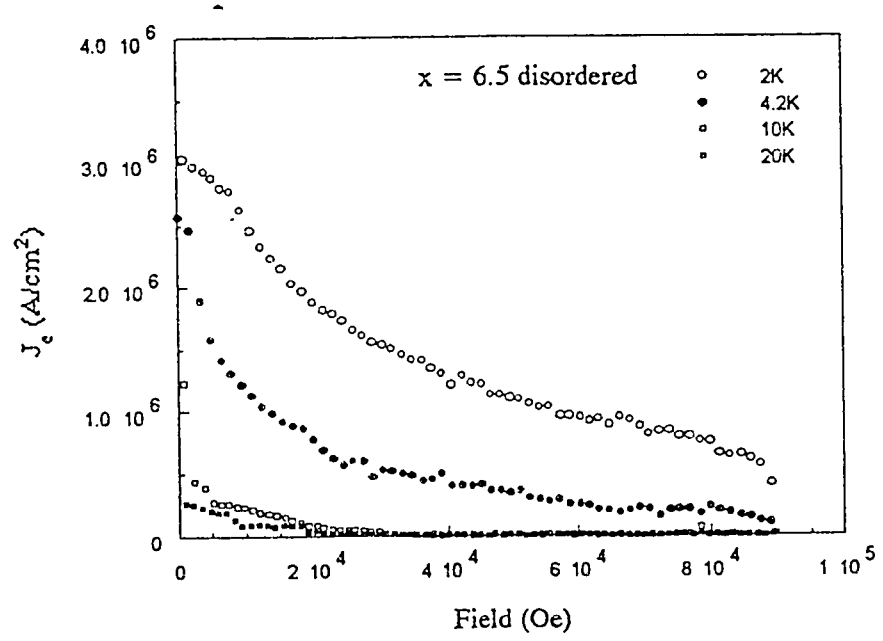

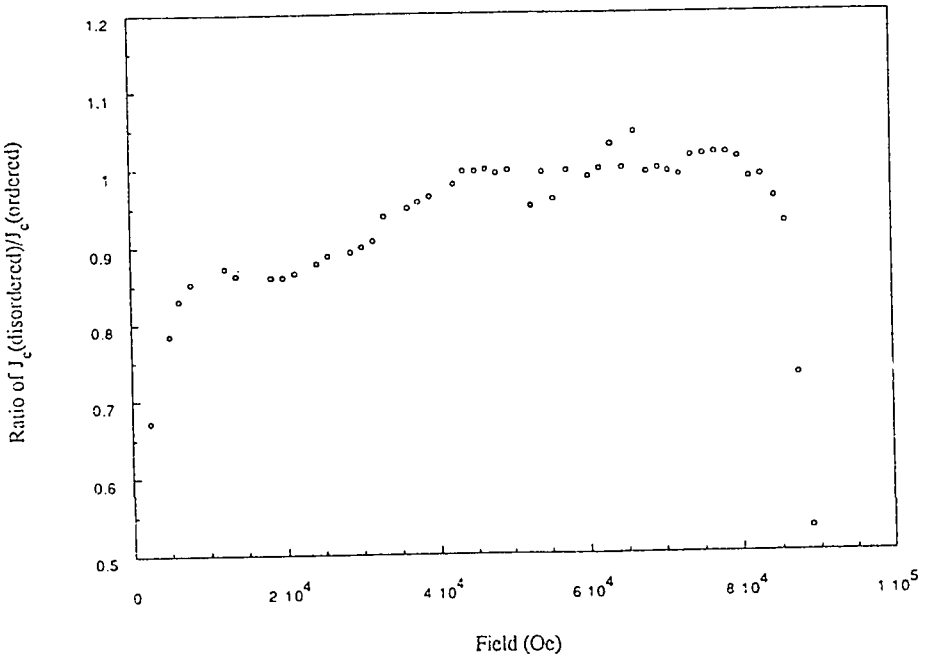

Figure 3.10: a) The field dependency of J_c for the disordered state at x=6.5 and b) the variation of the ratio of $\frac{J_c(disorder)}{J_c(order)}$ with the field.

Chapter 4

Energy Losses

4.1 Introduction

Although superconductors carry DC current without resistance, AC current or a changing magnetic field will lead to energy losses. These losses are small compared with the losses encountered in an ordinary copper wire at room temperature [8]. Low energy losses are the main attraction in any practical application of superconductors.

There are 3 main types of energy losses commonly encountered in type II SC [12]. These are: 1) surface loss generated by the movement of vortices in and out of the sample, 2) annihilation loss due to moving vortices in the opposite field direction and, 3) bulk pinning loss as vortices become unpinned (they jump between pinning centers in the bulk). The third type is often called hysteretic loss.

For HTSC, the losses are larger than that of conventional type II SC, even at very low temperature. These losses are mainly due to the bulk pinning losses caused by the irreversible motion of the magnetic fluxoid that interact with pinning centers. The hysteresis behavior of the magnetization of granular HTSC is discussed in section 3.1 for J_c behavior which will be used to explain the energy loss in HTSC. The main

features are summarized in the following section [44, 70, 11, 32] :

- For applied field $H_{ap} < H_{c1}^{w}$, field penetration does not exist and there are no flux lines generated. The grains are in the Meissner state and the magnetization is completely reversible, consequently there is no loss found.

- As H_{ap} is further increased above H_{c1}^{w}, flux lines penetrate the sample via the weakest links and drive them into the normal state. This gives rise to inter-granular loss which is dominant. In this region, the losses are proportional to the 4th power of H_{ap} for YBCO and the 7th power for GdBCO.

- At $H_{ap} > H_{c2}^{w}$, the inter-granular loss vanishes . The losses are mainly due to intra-granular loss which corresponds to the current surrounding the decoupled grains. In this region (up to $H_{ap} < H_{c1}^{grain}$) the losses remain nearly constant.

- Finally, at fields above H_{c1}^{grain}, the grains are decoupled. The vortex lines and the associated intra-granular currents propagate into the interior of the grains. The motion of these vortices gives rise to intra-granular losses. For YBCO, the losses exhibit almost 3th power dependency of H_{ap} up to a certain field above which they are saturated.

The above mechanism is different in conventional type II SC where losses are mainly due to surface losses [45]. Pauza et.al also found that in polycrystalline $YBa_2Cu_3O_{7-\delta}$, large inter-granular losses are due to the irreversible motion of Josephson vortices, while surface barrier and annihilation losses are neglected [53]. The Josephson vortices are generated by the coupling between the grains and contain no

normal core as in the conventional Abrikosov vortices [73]. These coreless Josephson vortices are assumed to be pinned at the intersection points of grain boundaries while the Abrikosov vortices are pinned at defect sites inside the grains. The motion of these vortices relative to their pinning centers leads to the major observed energy losses [46]. Moreover, the losses at large fields are determined by the size of the grains and not by the size of the sample [54].

Magnetic energy losses are conventionally measured by measuring the area of the hysteresis loop generated by cycling the applied magnetic field. The energy per unit volume per field cycle (W) being dissipated inside the superconductor is given as:

$$W = \int M(H_a) dH_a \tag{4.1}$$

where M is the magnetization and H_a is the applied field. To evaluate W, we may use the following expression for $M(H_a)$:

$$M(H_a) = \frac{1}{2V} \mid r \times J(r) \mid d^3r \tag{4.2}$$

where $J(r)$ is the current density distribution at distance r inside the sample and V is the sample volume [25].

The energy loss in type II superconductor as suggested by Bean is calculated from hysteresis loop (HL) area as in eqn.4.1. A brief introduction about this model has been treated in section 3.1. The calculated HL area is given as:

$$W = \frac{H_{ap}^3}{6\pi H^*}, \qquad H_{ap} \leq H^*(slab) \tag{4.3}$$

$$W = \frac{H_{ap}^3}{3\pi H^*} - 5\frac{H_{ap}^4}{16\pi H^{*2}}, \qquad H_{ap} \leq H^*(cylinder) \tag{4.4}$$

where H_{ap} and H^* are the external applied field and the first full penetrating field (to the sample center) respectively. H^* is related to J_c as

$$H^* = \frac{\pi J_c D}{5} \tag{4.5}$$

where D is slab thickness or cylinder diameter, while J_c is taken to be $\pm$ constant or 0. In our cases, all the samples are in slab forms which give the D as samples thickness (for single crystal samples) or as average grain size (for polycrystalline samples: D$\approx$15 μm). The D values is given in table 2.

In a granular superconductor, as explained above, $J(r)$ is the sum of the inter- and intra-granular currents, namely $J_j(r)$ and $J_G(r)$. Therefore, the magnetization M and energy loss W are the sum of their inter- and intra-granular terms labelled as j and G respectively.

Recently, Brandt and Indenbom [6] and Zeldov et.al. [72] derived an expression for $M_j(H_a)$ by assuming that the current density is field independent. Their result is then used by Muller et.al [?] (in eqn.4.1) who derived the intergranular hysteresis loss as :

$$W_j = 2\pi\mu_o \frac{a}{d} H_d H_m \left[-\tanh\left(\frac{H_m}{H_d}\right) + 2\frac{H_d}{H_m} \ln\left(\cosh\left(\frac{H_m}{H_d}\right)\right)\right] \tag{4.6}$$

where a, d, H_m, H_d are the half width of the sample, thickness, field amplitude, and characteristic field[4] , respectively. They then assumed that intra-granular critical

[4] $H_d = \frac{dJ_c}{\pi}$

current density $J_{c,G}$ is independent of the local magnetic field inside the grains. The intragranular hysteresis loss is obtained as:

$$W_G = \mu_o \frac{4H_m^3}{3H_G^*}\left(1 - \frac{H_m}{2H_G^*}\right) \tag{4.7}$$

where H_G^* is the first full penetrating field (to the grain center). It should also be noted that equation 4.7 for intergranular loss has a similar behavior as that found in eqn.4.4 obtained in Bean's model.

For the following sections, we will discuss our energy losses results on single and polycrystalline YBCO and compare them with the expected behavior from Bean's model.

4.2 Results and Analysis

4.2.1 Energy losses in $YBa_2Cu_3O_{7-\delta}$ single crystal

In our investigation, we measure energy losses as a function of the applied magnetic field up to 90 kOe and for FC and ZFC states. We examine energy losses for field parallel and perpendicular to the c-axis of the single crystal. The calculated expected behavior from Bean's critical state model is also presented by using eqn.4.3.

For FC or ZFC states, our results are shown in Fig. 4.1 and 4.2 presented on log-log scales. The applied fields are in the range of $H_{ap} > H_{c1}^{grain}$ so that the dominant behavior is the intra-granular loss.

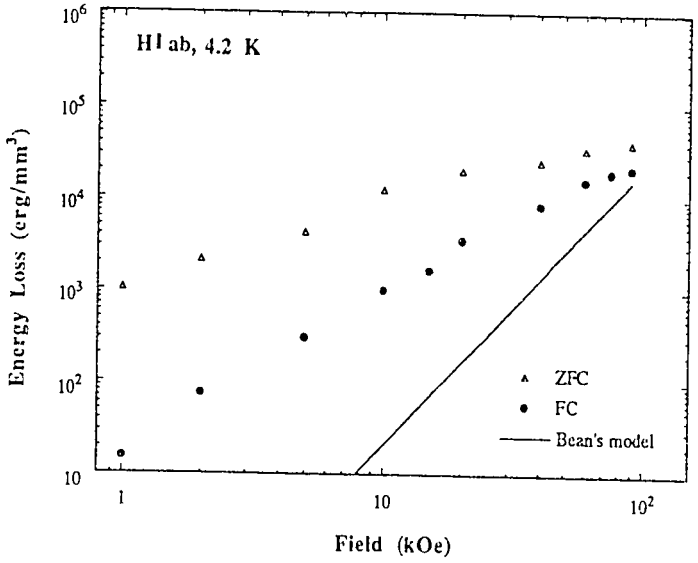

Figure 4.1: The hysteresis losses of single crystal YBCO at 4.2 K and with field applied parallel to the ab-plane.

In Fig.4.1, we present the energy losses at 4.2 K for field applied parallel to ab-plane of the sample. At lower fields, it is observed that the ZFC loss is greater than that of the FC by about two order of magnitude. However, the difference decreases

with increasing field and reduces to about a factor of 3 at about 90 kOe.

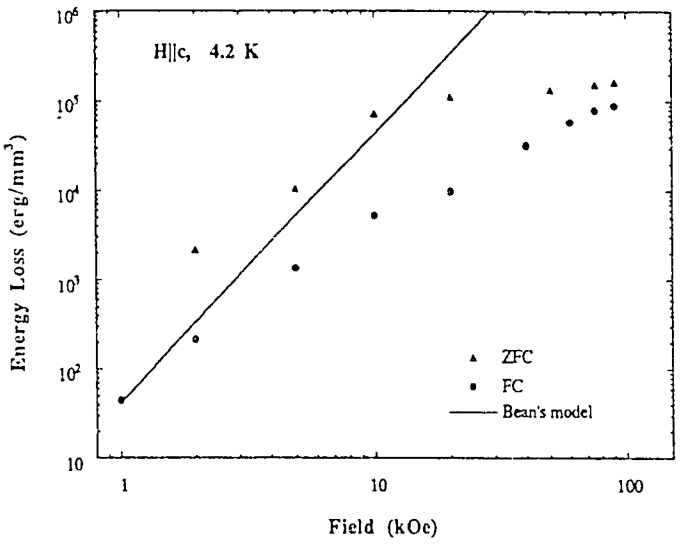

Figure 4.2: Hysteresis losses on single crystal YBCO at 4.2 K and with a field applied parallel to its c-axis.

In comparison with Bean's model, both values of energy losses approach the values expected from Bean's model at $H \gtrsim 70$ kOe. At low fields, the results are in sharp disagreement with Bean's model. Above 20 kOe, the experimental data approach saturation gradually, unlike what is expected from Bean's model where losses increase without approaching saturation.

It is also observed that both losses increases linearly (on a log scale). The ZFC energy losses has a lower slope (almost half) than that of the FC. The initial slope values obtained by linear fit are presented in table 3 for single and polycrystalline samples. These slopes are much lower than that predicted by Bean's model indicating a weaker field dependency of the energy loss. For H parallel to ab-plane, W_{ZFC} and W_{FC} are proportional to $H^{0.83}$ and $H^{1.6}$ respectively.

In Fig4.2, we present energy losses produced by cycling the field parallel to the c-axis of the crystalline sample. The initial ZFC loss exceeds the FC loss by an order of magnitude up to 20 kOe above which the difference between ZFC and FC losses decreases rapidly. Both saturate nearly to the same maximum value near 90 kOe. The ZFC saturates earlier (at about 10 kOe) than the FC which saturates near 80 kOe.

The ZFC and the FC hysteresis losses increase linearly with almost the same slopes with the ZFC curve lying above the FC curve. In comparison with the Bean's model, both the FC and the ZFC losses have initial slopes of n=1.7 and 1.8 respectively, which are different from what is expected from Bean's model (n=3).

There is an initial linear increase followed by a gradual increase as observed in Figs.4.1 and 4.2. This gradual increase can be attributed to the absence of granularity or intergranular dissipation in the single crystal. The losses are mainly caused by irreversible motion of flux lines inside the crystal. In other work on melt textured YBCO it was demonstrated that no inter-granular losses exist at a field below H_{c1} [70]. Therefore, the field at which the losses saturate may be related to the field of full penetration in the superconducting sample.

It is also found that the losses for $H_{\|ab}$ are smaller than those with $H_{\|c}$.(about a factor of 5 at saturated values for FC and ZFC). These results are in qualitative agreement with those of Zanella et.al. for melt textured samples [71]. This anisotropy can be possibly attributed to the higher J_c values along the c-axis.

It is noticed that for both cases ($H_{\|c}$ and $H_{\|ab}$) that ZFC losses are higher than that of FC. Larger losses are related to wider hysteresis loops, and correspondingly,

higher J_c values. More pinning is usually associated with higher J_c, leading to more trapped flux/vortices. In other words, the relative motion of Abrikosov vortices to their pinning centers will give rise to a higher intra-grain energy losses. We proposed that this case is an indication that ZFC states are less ordered than FC. Possible relevancy to remanent magnetization will be discussed in the next chapter.

4.2.2 Energy Losses in Polycrystalline $YBa_2Cu_3O_{7-\delta}$

In our energy losses investigation for polycrystalline $YBa_2Cu_3O_{7-\delta}$, the magnetic field measurements were performed in a field as high as 90 kOe and for FC and ZFC states. The expected behavior from Bean's critical state model is also presented using eqn.4.3 with D taken as the average grain size which is 15 μm. Our results on the as-prepared sample are presented in Fig.4.3 on log-log scales.

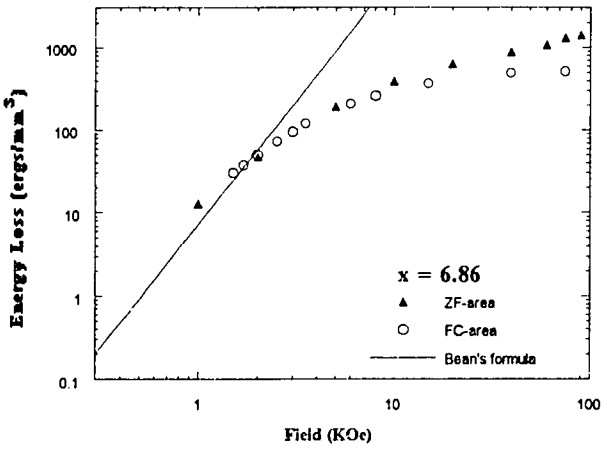

Figure 4.3: Energy losses for the as-prepared polycrystalline $YBa_2Cu_3O_x$ with x=6.86.

The results showed that FC and ZFC losses initially merge, then both linearly increase with field (slope n=1.67, see table 3). Both change slopes and diverge from each other near 4 kOe approaching saturation gradually. The FC curve saturates at about 500 ergs/mm^3, while the ZFC curve increases slowly and reaching about 1.5 kergs/mm^3 near 90 kOe. The Bean's model is in fair agreement with initial slopes of

FC and ZFC losses up to 2 kOe.

In comparison with the single crystal results, the saturated energy losses found in ZFC and FC curves of the single crystal sample is about two order of magnitude higher than the losses found for polycrystalline $YBa_2Cu_3O_{7-\delta}$ (high field losses). Both single and polycrystalline samples posses an initial linear increase with varying slopes that changes with increasing field. For polycrystalline material, this initial losses may be related to the initial sharp drop of J_c and both samples are related to the irreversible behavior of the magnetization. A drop of J_c might be responsible for an increase of energy loss. However, for single crystal results, it is almost constant up to very high field ($\sim 6T$) above which J_c starts decreasing rapidly. Moreover, the initial slopes found in the FC state for single and polycrystalline samples are very close to each other, while the ZFC results showed varying results (see table 3).

On the other hand, the single crystal FC and ZFC for $H_{\|c}$ have similar slopes and approach the values expected from Bean's model at low fields. While for $H_{\|ab}$, the ZFC and the FC measurements have different values.

It was also found that the polycrystalline results saturate earlier at lower field than that of the single crystal. The field at which the losses approach saturation is possibly attributed to the first full penetrating field ($H^* = \frac{2\pi}{c} D J_c$) discussed in Bean's model. Because of the smaller size of the polycrystalline grains compared to the size of the single crystal sample, a smaller H^* is needed. Consequently, earlier saturation is observed for the polycrystalline results.

The saturated values of the single crystal ($\sim 10^5$ ergs/mm^3) are greater by about 2 orders of magnitude. This behavior is due to the intra-granular behavior of the

polycrystalline sample. Thus, it confirms the previous results of J_c of the single crystal $YBa_2Cu_3O_{7-\delta}$ which is smaller than that of the polycrystalline (also about 2 orders of magnitude).

Oxygen Stoichiometric Effect

The following figures (Figs.4.4 and 4.5) illustrate the field dependency of energy losses on polycrystalline $YBa_2Cu_3O_x$ in different oxygen content. The expected behavior from Bean's critical state model is also presented with the value of D taken as the average grain size which is 15 μm and it is assumed to be independent of oxygen content. All results are presented on log-log scales.

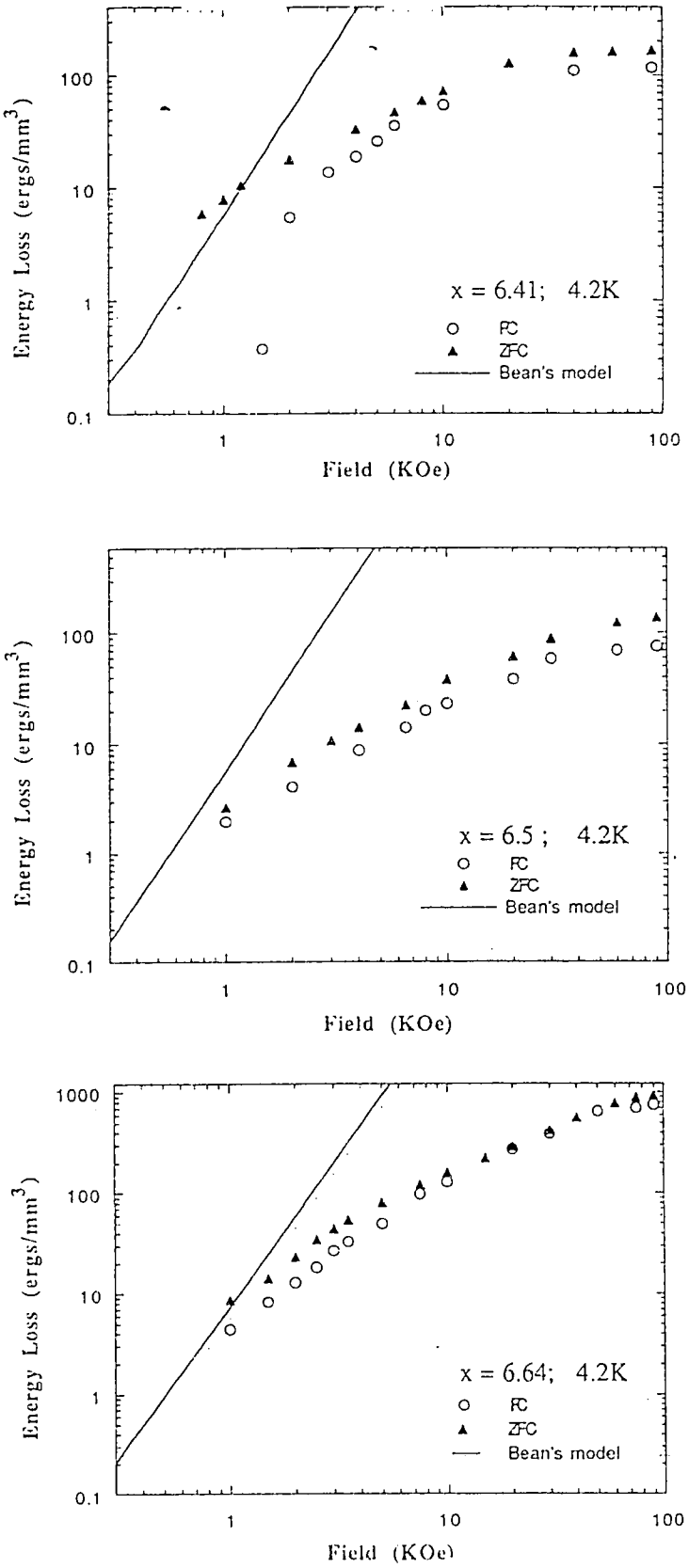

Figure 4.4: The field dependencies of energy losses at different oxygen content of polycrystalline $YBa_2Cu_3O_x$ with (a) x=6.41 (b) x=6.5 and (c) x=6.64

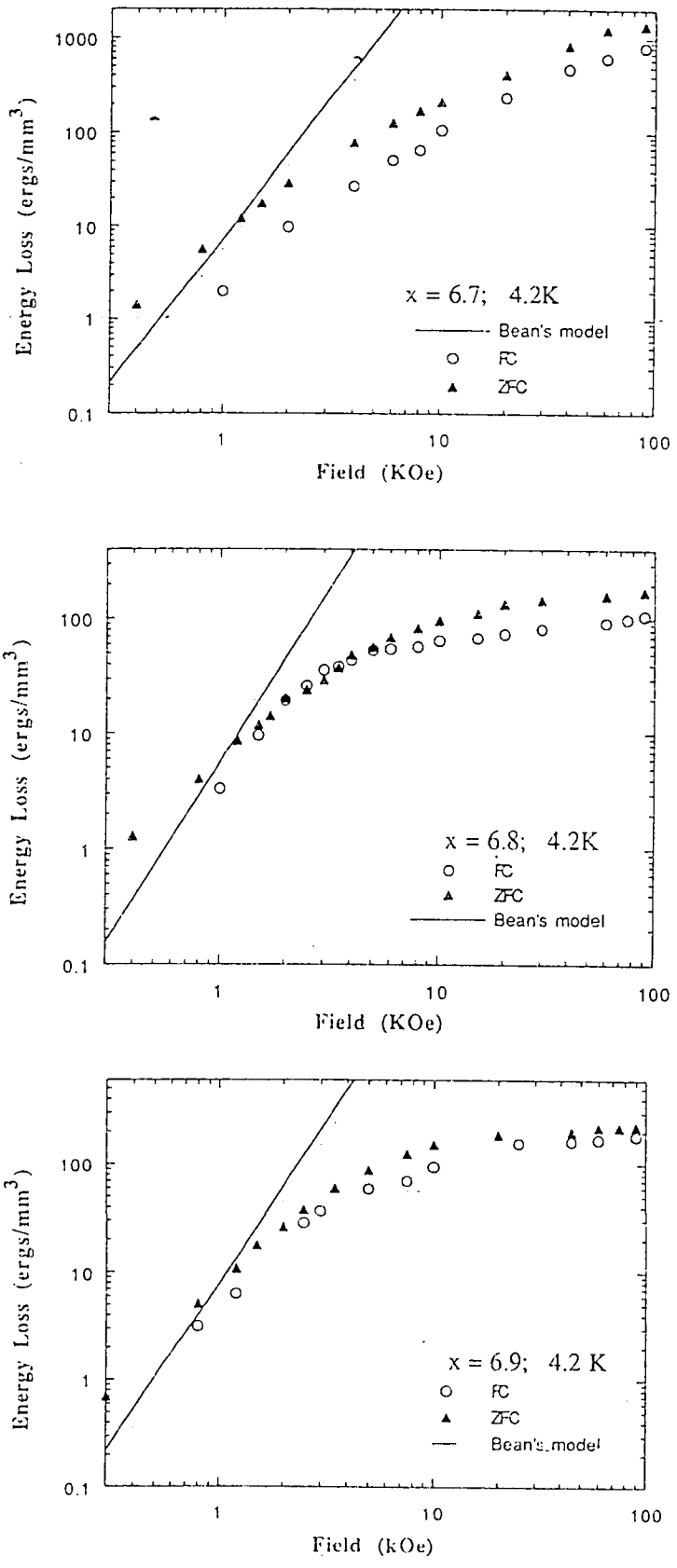

Figure 4.5: The field dependencies of energy losses at different oxygen content of polycrystalline $YBa_2Cu_3O_x$ with (a) x=6.7 (b) x=6.8 and (c) x=6.9

Table 3.

The initial slopes of Energy losses curves

samples:	ZFC slope	FC slope
Bean's model	3	3
single crystal:		
H‖ab	0.83	1.59
H‖c	1.8	1.76
polycrystalline:		
as prepared (x=6.86)	1.67	1.63
x=6.41	0.98	1.6
x=6.5	1.14	1.2
x=6.5 (disordered)	1.16	1.35
x=6.64	1.44	1.54
x=6.7	1.58	1.67
x=6.8	1.9	1.75
x=6.9	1.9	1.92

Generally, the curves on Figs.4.4 and 4.5 can be divided into 2 regions. The first initial region shows an almost linearly increasing behavior which may be related to the sharp drop of the initial J_c curves. The second one is the weakly field dependent energy loss which exhibits the saturated values. The transition region between the first and the second regions is attributed to the first full penetrating field H_p^g, which Xu Y. has interpreted it to be twice of H_p^g [69].

The slopes in the first region obtained by linear fit are presented in table 3. As the oxygen content increases, these slopes increase linearly without a pronounced difference between the ZFC and the FC results. The increase of slope is an indication of stronger field dependency of oxygen rich samples. The highest slope (n=1.9), for example, gets closer to the expected behavior from Bean's model (n=3). On the other hand, Xu M. et.al. observed an n≈3 at this range for polycrystalline DyBaCuO samples, thus confirming the expected behavior of Bean's model [42]. The discrepancies between our results and Bean's model could possibly be due to the strong pinning forces of our samples [5] .

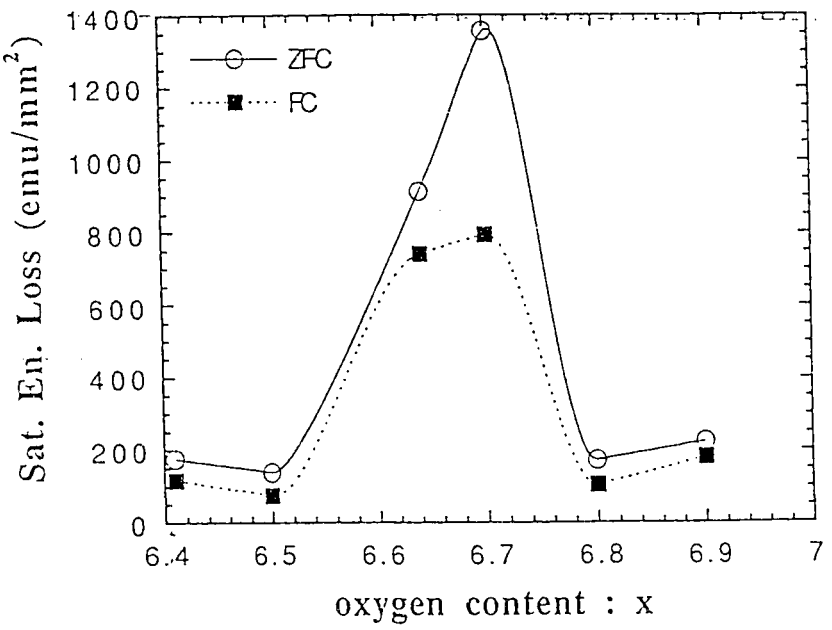

Figure 4.6: Maximum (or saturated) energy losses vs oxygen content in polycrystalline $YBa_2Cu_3O_x$.

[5] Recently, Muroi et.al. [49] argued that cation substitution (Y —> Dy) near the CuO_2 plane could affect the T_c by changing the hole concentration which may also change the losses behavior.

The maximum or saturated energy loss values (taken at 90 kOe), if plotted versus the oxygen content x as in Fig.4.6, remains almost constant with increase in x until around 6.5 where a sharp increase is observed. The saturated value starts to go down after reaching a peak of 13.5 kergs/mm^3 for the ZFC measurements (the FC value is half of this at x=6.7). It again started a rather sharp increase at 6.8 and reached the second peak at 6.86 with the FC data corresponding to $\frac{1}{3}$ of that for the ZFC which rapidly drops at 6.9. This figure doesn't exhibit a linear behavior as the case of $J_c(x)$. The ZFC curves lies above that of FC as the case of single crystal and as prepared polycrystalline samples, confirming a more ordered state of FC.

An interesting feature is present on Fig.4.6. It is the occurance of a peak observed at x=6.7 . Another peak at x=6.86 is possibly related to an anomaly of high J_c(x=6.86) which is caused by the different heat treatment. The reasons that oxygen deficiency might increase the pinning seems unfounded since a higher pinning will slow the vortex and in turn generate a smaller loss. Also the first peak observed at x=6.7 has complicated this issue making it difficult to relate $J_c(x)$ to the energy loss behavior for different x values.

However, if we relate this behavior to the two plateaus observed on $T_c(x)$, a better understanding can be achieved. The first peak might be due to the first $T_c(x)$ plateau at which a stagnation in the number of charge carrier (holes) doped to CuO planes occurs at x=6.6, while the second peak is related to the second plateau of $T_c(x)$ which is due to a saturation effect of T_c.

Oxygen Disorder Effect

In Fig.4.7 we present the energy losses for the maximum disordered state associated with x=6.5. Here the FC and the ZFC losses are observed to increase linearly with field. The initial linear slopes of FC extends up to 30 kOe, while for the more ordered state it extends only up to 10 kOe. Also a slightly larger n of the disordered state reveals that the losses are more strongly field dependent.

In the previous chapter, the disordered J_c behavior observed at 4.2K is half of the ordered value at low field, and almost the same value at higher field. Oppositely to the J_c behavior where the energy loss of the disordered state has almost similar initial behavior as the ordered state. However, its saturated values, i.e.180 and 280 ergs/mm^3 for the FC and ZFC respectively, appear to be twice that of the ordered values. This behavior seems to be a new feature. The absence of O(1) atoms from their natural sites (which are free to move to the neighboring area) generates higher losses at high field. Also, microscopically we can argue that the dynamic of the Abrikosov vortices are similar in both states.

In comparison with Bean's model, the disordered results appear to have sharp disagreement at a field above 10 kOe. Moreover, similar initial slopes for ordered and disordered states showed that the general field dependency of the energy loss was not affected much.

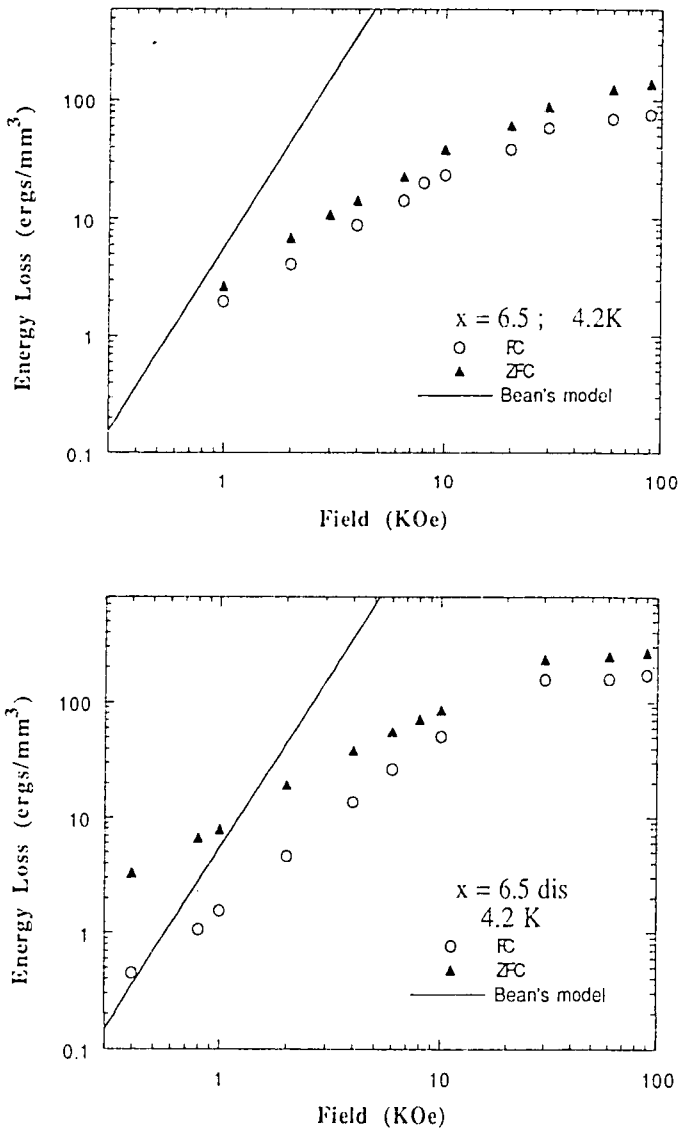

Figure 4.7: The field dependencies of energy losses at oxygen ordered (a) and disordered states (b) of polycrystalline $YBa_2Cu_3O_x$.

Chapter 5

Remanent Magnetization

5.1 Introduction

When a magnetic field above the lower critical field H_{c1} is applied to a type II SC, lines of magnetic flux then penetrate into the bulk of the sample. Generally, when the magnetic field is removed again, some of the flux remains trapped within the bulk showing a positive magnetic moment. This trapped flux often referred to as the remanent moment M_R. It is defined as the remaining moment in the sample obtained by turning off the field after magnetizing the sample by either ZFC or FC methods. Two processes contribute to this flux trapping mechanism for granular type II SC, namely : the pinning of Abrikosov vortices within the grains and the inter-grain voids associated with weak links between grains. [29]. The former is known to strongly influence the critical current which generate the hysteretic behavior of the sample, while the latter has a strong dependence of critical current on the applied field.

The remanent magnetization has also been related to the presence of persistent supercurrents around the perimeter of the ceramic SC rings [39]. Several scientists

have measured the field directly inside ceramic toroids of HTSCs and confirmed the presence of persistent currents [39]. Grader et.al. detected a slow decay of the persistent current indicating a flux creep [20]. The decay time for about 12 days in liquid nitrogen and zero field has been reported [67]. Leiderer et.al. also found that the remanent magnetization arised simply from the trapped flux [36].

The remanent magnetization is also related to the strength of flux pinning and depends intrinsically on both temperature and applied field [42]. Different pinning mechanisms, anisotropy, and a short coherence length are a few feature which make this subject complex. However, a qualitative understanding can be built by the scattered reports that we have collected as follows.

The field dependency of M_R, as reported by Y.Xu et al. [69] and M.Xu [42], has 3 plateaus for disk and hollow shaped YBCO (on logarithmic plot) . These plateaus are interpreted as follows, in terms of granular theory in type II SC as discussed in the previous chapters.

- The first plateau which gives $M_R = 0$ indicates a complete Meissner effect in the range of $H_{ap} < H_{c1}^{w}$ (the weak link critical field).

- At $H_{ap} > H_{c1}^{w}$, M_R increases with H_{app}^{m} (m is about 3 to 5). This means that the field penetrates deeply into the boundary between the grains in the form of vortices. At the same time, a shielding current is surrounding each grain preventing further penetration inside the grains. As a result, more vortices are trapped at the inter-grain voids.

- The remanence then reaches the second plateau in fields closer to the lower

critical field of the grains: H_{c1}^{grain}. In this region, the Lorentz force far exceeds the pinning force of the inter-grain voids. The vortices then move freely in the boundary between the grains but are still unable to penetrate into the interior of the grains.

- For $H_{app} > H_{c1}^{grain}$, flux starts to penetrate inside the grains. The penetration increases gradually reaching a third plateau at about $2H_p^g$ (the field of full penetration of the grains). At this third plateau, the remanent moment increases slowly with field and is considered to be saturated.

For the temperature dependency of M_R, Laiho et.al reported for YBCO samples, that M_R increases first with temperature, reaching a peak at 15 K, then gradually decreasing and vanishing at a temperature less than the T_c [35]. The decrease is non-exponentially as it was noticed first on HTSC by Muller et.al.[48]. In other work, Lahderanto et.al. [33] observed a partial reversibility of M_R. This behavior was observed when a sample in a trapped flux state was heated up in a zero external field to a temperature below T_c , upon cooling, it retained its original trapped flux state.

In other work the temperature dependency of M_R in low fields is proposed to follow a simple relation all the way up to T_c [68, 15]:

$$M_R(T) = M_{FC}(T) - M_{ZFC}(T) \tag{5.1}$$

Malozemoff et.al. verified the above equation in both ceramic and bulk crystal $YBa_2Cu_3O_7$ [38]. However, this relation originates from a phenomenological result for spin-glasses and has a limited range of validity [14]. It is restricted to low fields

(< 500 Oe) and low temperatures (near to 4.2 K).

The first attempt (and probably the simplest) to describe this remanent magnetization behavior is the Bean's model proposed in the early sixties. A brief introduction of this model has been given in Chapter 3. Bean found that the geometrical size dependence between the remanent and J_c namely,

$$M_R = \frac{J_c D}{40} \qquad slab \tag{5.2}$$

$$= \frac{J_c R}{30} \qquad cylinder \tag{5.3}$$

where R and D are radius of the cylindrical and thickness of the slab samples respectively. Yeshurun et.al. found that M_R increases linearly with grain size up to sizes of the order of a few hundred micrometers and becomes sublinear at larger sizes [68].

For the following sections , we will discuss our remanent magnetization results on single and polycrystalline YBCO and present them in terms of the total flux.

5.2 Results and Analysis

5.2.1 Single Crystal

a) ZFC state

Cycling the applied magnetic field (at a fixed temperature) from zero to a certain maximum and back to zero produces half a hysteresis loop. On this loop, two data points are used to obtain the variation of the remanent magnetization with H. These points are: the remnant moment M_R (known as isothermal remanent moment: IRM) , the point at zero applied field after reducing the field from its maximum value, and the maximum applied field H_{ap}^{max}. Repeating the similar process for a different H_{ap}^{max}

sequentially up to our maximum field, we have obtained the results shown in Figs.5.1 for the locuse of total flux ($M_R \times area$) vs H_{ap}^{max}.

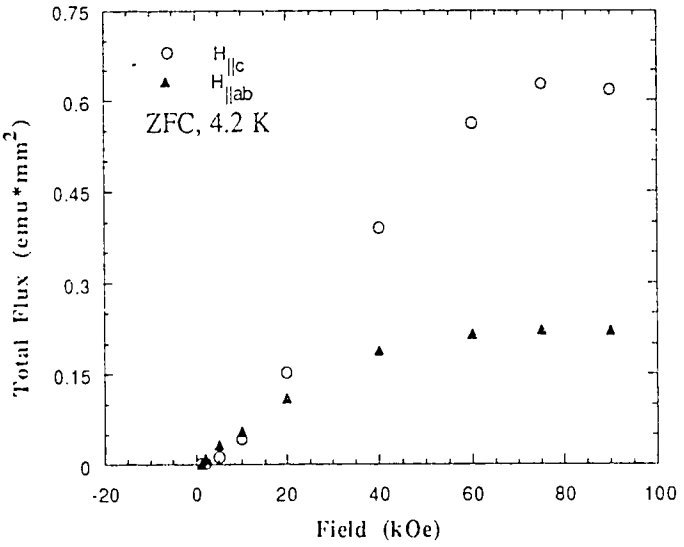

Figure 5.1: The total flux of single crystal YBCO at ZFC state for an applied field parallel and perpendicular to the ab-plane.

When the field is parallel to the ab-plane, the trapped flux i.e. IRM(ab) initially increases with concave downward behavior showing no threshold. At about 50 kOe, the curve reaches saturation. However, the IRM(c) curve initially increases rapidly with concave up behavior, crossing the IRM(ab) at 15 kOe. This is followed by concave down behavior with an inflection point at about 25 kOe. The curve then saturates at about 60 kOe which indicates a high (full) penetrating field H* as pointed out by McElfresh [41]. The saturated value of IRM(c) (0.65 emu-mm^2) is almost 3 times higher than that of IRM(ab) (0.22 emu-mm^2).

The ratio of IRM(c) / IRM(ab) (Fig.5.2) reflects the anisotropy of the pinning

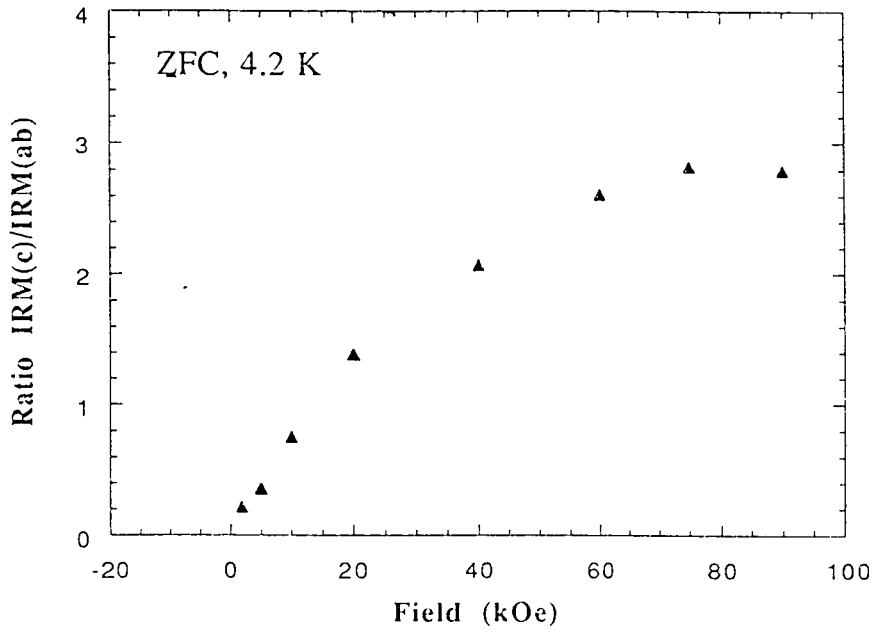

Figure 5.2: The variation of the ratio of $\frac{IRM(c)}{IRM(ab)}$ with the field.

forces along the c and ab-planes. This anisotropy then becomes more pronounced above 30 kOe and gives a value of almost 3 at 90 kOe. It illustrates that the fluxes are initially difficult to trap in the c-axis direction. However, as soon as the field increases above a threshold field (about 20 kOe), it is easily trapped along c-direction. On the other hand, in the ab-direction, the flux is easier to trap but it does not reach the same saturation value as reported along the c-axis.

The higher IRM(c) value is strongly related to a higher J_c indicating stronger pinning forces, and smaller losses associated with the c-axis as discussed in the previous chapters. Since the remnant magnetization is also related to the strength of the flux pinning we could draw the conclusion that stronger pinning is exhibited in the c-axis.

b) FC state

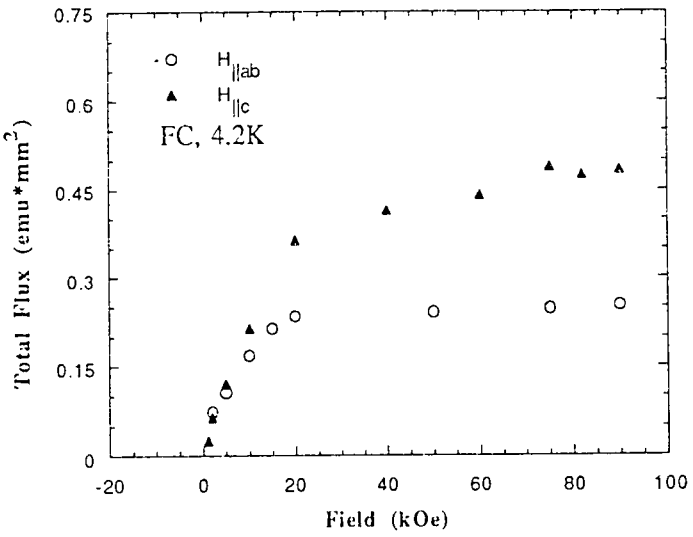

Figure 5.3: The total flux of single crystal YBCO at FC state for an applied field parallel and perpendicular to the ab-plane.

In the FC state, the field H_{cool} is applied at $T>T_c$, then cooled to T=4.2 K (the measurement temperature). The applied field is then swept to zero to obtain the remnant moment $M_R(H_{cool})$ in the FC mode (known as the thermo remanent moment: TRM). To obtain another pair of data, the temperature can be increased to $T>T_c$ to destroy the TRM, before cooling the sample in another field. The process is then repeated for different H_{cool} applied in the direction parallel to the ab-plane or to the c-axis of the single crystal. The results of such measurements are shown in Fig.5.3 in the form of total flux ($M_R \times area$) vs H_{cool}.

Initially, both TRM(ab) and TRM(c) increase with concave down behavior. At

20 kOe, TRM(ab) saturates, while TRM(c) continues to increase and saturates at about 60 kOe reaching 0.45 emu-mm^2, almost twice that of TRM(ab).

The ratio of TRM(c) over TRM(ab) is initially small, then the anisotropy becomes more pronounced at above 20 kOe and gives a value of almost 2 at 90 kOe. This observation confirms the ZFC results which indicate that a stronger pinning is exhibited in c-axis direction. However, both TRM curves saturated at a lower field than the corresponding ZFC curves. The saturated values of TRM at 90 kOe are also observed to be smaller than that of IRM. The above discrepancies seem to be in agreement with the proposed explanation on energy losses which pointed out that the ZFC state is less ordered than the FC state.

Similar remanent magnetization measurements have been performed for polycrystalline YBCO samples with different oxygen contents. These results are reported in the following sections.

5.2.2 Polycrystalline Total Flux

The remnant magnetization investigation of polycrystalline YBCO has been done for the FC and the ZFC states. Our result on as prepared sample are presented in Fig.5.4 in the form of total flux vs H_{ap}^{max}.

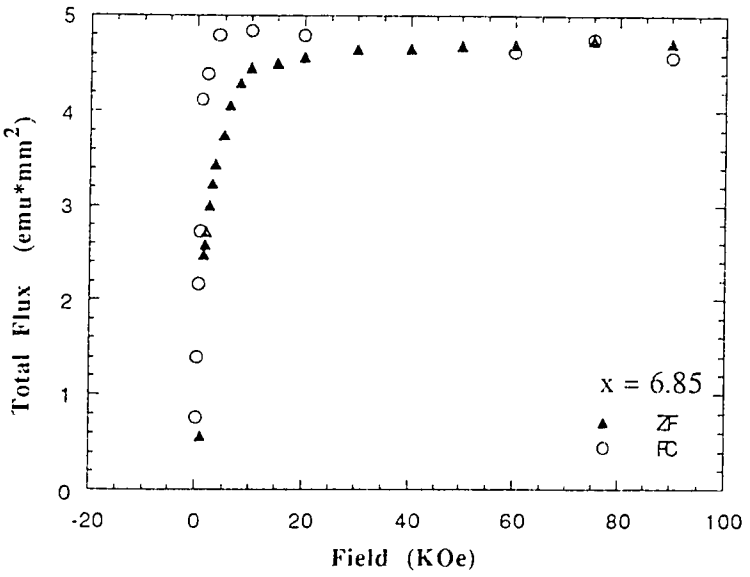

Figure 5.4: Total flux for the as-prepared polycrystalline YBaCuOx with x=6.86.

A concave up increasing behavior is observed for the initial curve of ZFC followed by a concave down gradual increase with the inflection point at 2.0 kOe. At 5 kOe the curve reaches saturation. A faster initial increase is observed for FC with an inflection point at about 1 kOe to 3 kOe above which the curve gradually saturates. At 7.5 kOe the saturated FC curve merges with that of ZFC at a value of 2.4 emu-mm^2.

In comparison with single crystal results, the saturated values of the total flux of the polycrystalline samples are observed to be greater than that for the single

crystal by about an order of magnitude. The polycrystalline results are also observed to saturate earlier (at lower field) than that for the single crystal. This difference confirms the previous results on J_c and energy losses that attributed to the absence of granularity in the single crystal. The field when the remnant moment started to saturate is attributed to the first full penetrating field (H*) [41, 42] at the sample center for a single crystal or the center of a grain for a polycrystal.

Oxygen Stoichiometric Effect

The following Figs.(5.5 and 5.6) illustrate the field dependency of M_R for polycrystalline YBCO with different oxygen content. The magnetic field measurements were performed on the FC and the ZFC states. All the results are presented in the form of total flux vs H_{ap}^{max}.

Generally, the curves in these Figs.(5.5 and 5.6) can be divided into two regions. The first, initial region, indicates an increase in the trapped flux. The second region shows the saturated behavior of the total flux. The transition region in between could possibly be due to the first full penetrating field.

In the first region, it is observed that the ZFC curves increase with concave up behavior followed by concave down behavior with inflection points shifted from 0.5 kOe at x=6.41 to about 2 kOe at x=6.9. A plateau, which extends between 1.8-3.5 kOe has been observed at x=6.8 for which we have no explanation. A different behavior of the ZFC curve is observed for x=6.86 (the as-prepared sample) which gives an almost linear increase with field. The initial FC curves exhibit a concave down behavior, then reaches the saturation values at about 3 kOe. As a result, the FC curves initially, lie above those for the ZFC then crossover at a field in between 3 to 9 kOe. An exceptional behavior occurs at x=6.41, where it first reaches a maximum value at 2 kOe, then decreases rapidly crosses over the ZFC curve at 5 kOe to attain its saturated value at 40 kOe.

In the second region, the FC curves are observed to saturate earlier with smaller

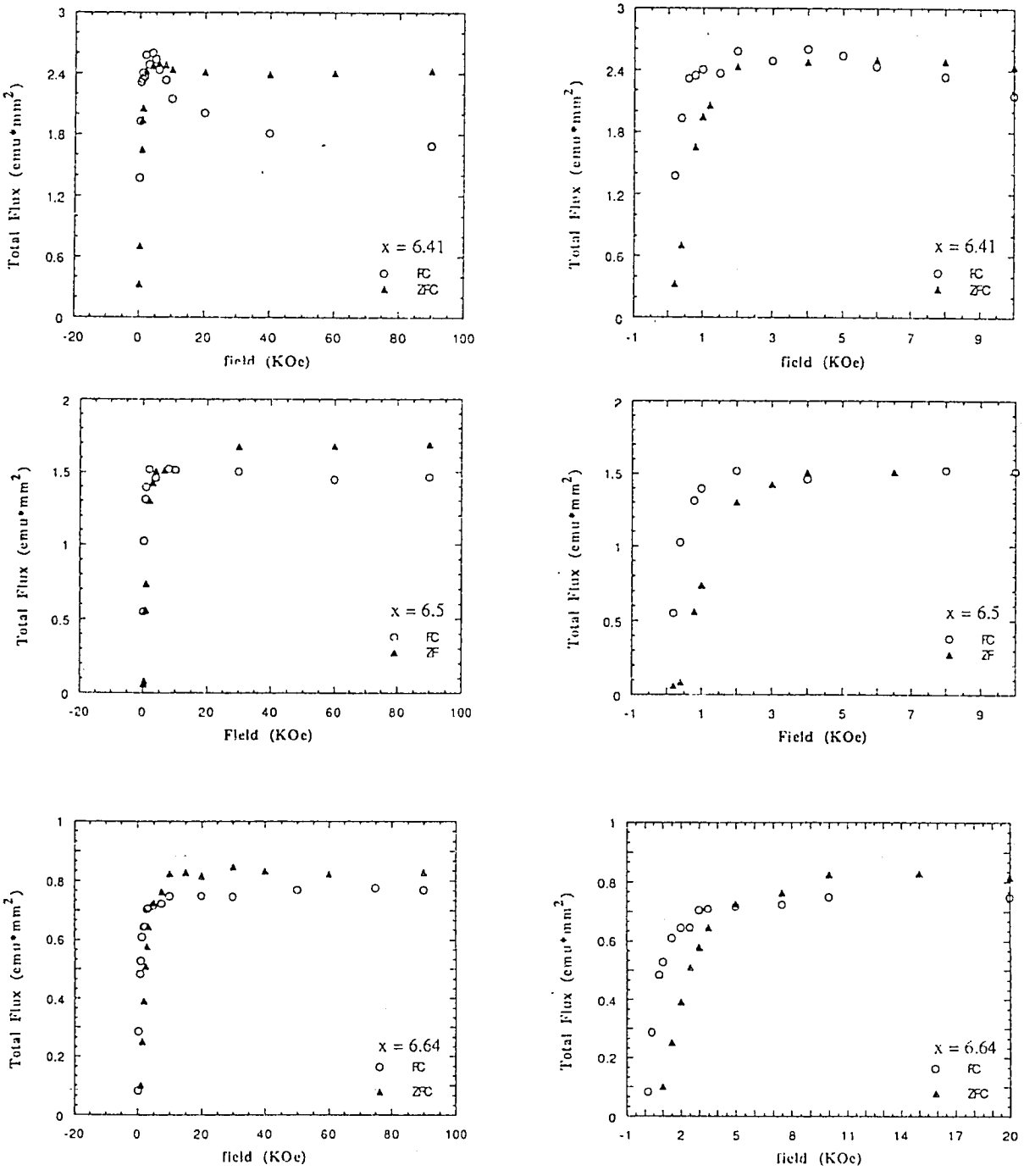

Figure 5.5: The field dependencies of total flux at different oxygen contents of polycrystalline $YBa_2Cu_3O_x$ where a)x=6.41 b)x=6.5 and c)x=6.64

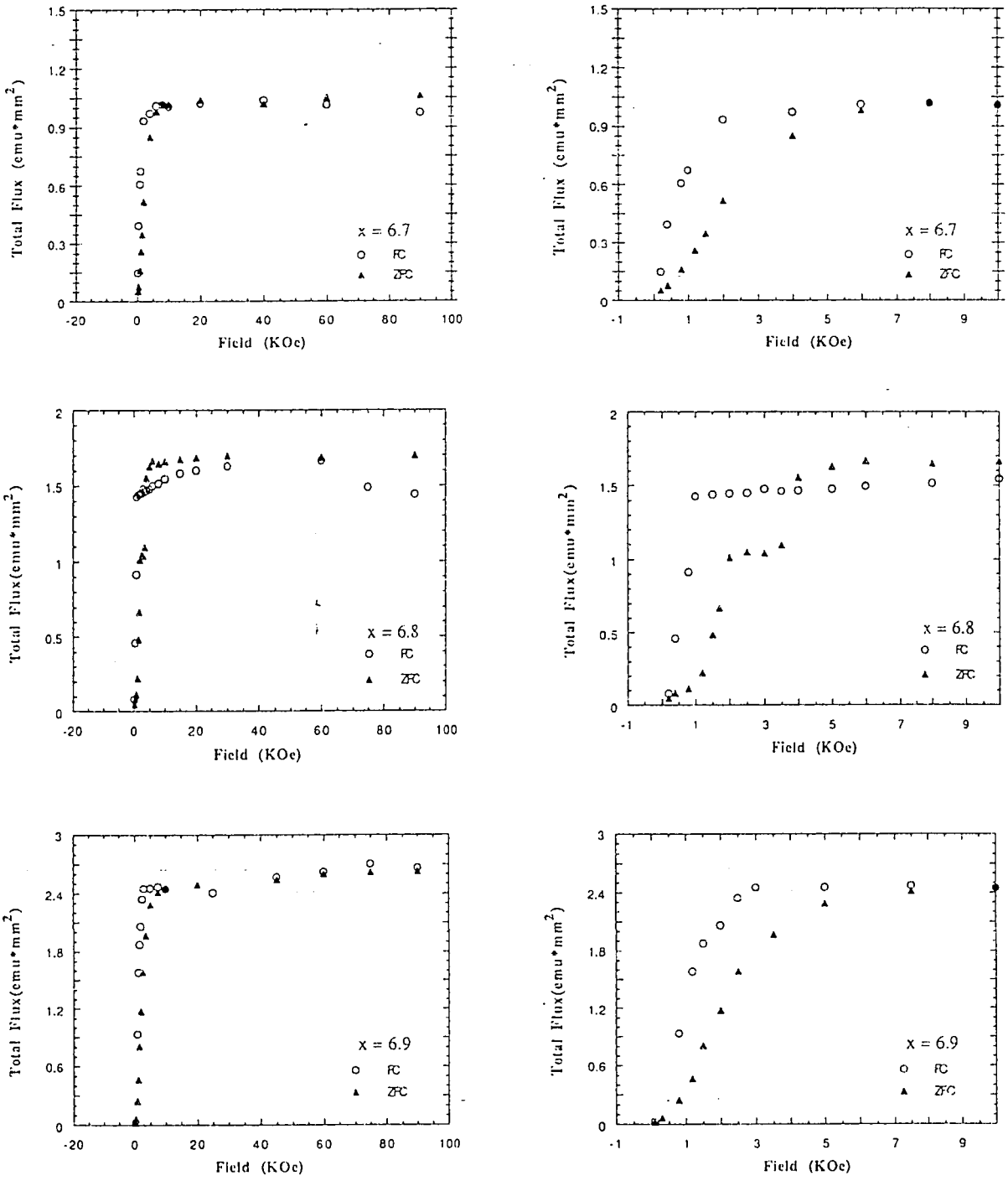

Figure 5.6: The field dependencies of total flux at different oxygen contents of polycrystalline $YBa_2Cu_3O_x$ where a)x=6.7 b)x=6.8 and c)x=6.9

saturated values than that of the ZFC. The saturated values of the FC and the ZFC curves at 90 kOe, for different oxygen contents, are presented in Fig 5.6b As the oxygen conten increases, the saturated values decrease, reaching a minimum at x=6.64 and the increase again. An exceptionally high value is exhibited at x=6.86 (for the as-prepared sample). This V-type behavior with the maximum at the ends and minimum at x=6.64 illustrates the strength of the pinning of the Abrikosov vortices at high field (90 kOe). The minimum is possibly related to a plateau in $T_c(x)$ and a peak in energy losses W(x). Analogically, the stagnation of the number of holes doped to the CuO plane may be responsible for this minimum.

The maxima at the end could be explained in terms of large number of O(1) vacancies at x=6.41 that produces additional pinning and a more pronounced effect in $M_R(x)$. The other maximum in the oxygen rich samples (x>6.8) may be due to the strong pre-existing pinning and the dominated factor of a highly transferred charge carrier.

The less dominant contribution of additional pinning to the energy loss and J_c is related to the charge transfer (CT) model. The absence of O(1) atoms in the chain reduces the charge carriers transferred to the CuO plane. At the same time, it is also generating vacancies which provide additional pinning. In summary, the O(1) vacancies reduce the effect of charge transfer which are known to dominate the behavior of $J_c(x)$ and W(x), while the vacancies also provide additional pinning which dominate the $M_R(x)$ behavior.

Another factor which may be responsible for the degradation of $M_R(x)$ as x decreases to 6.64 (from 6.9) is the effect of low temperature (600°C) annealing of the

samples. This kind of annealing was believed to reduce the amount of pre-existing pinning [51]. A more detailed study of the effect of annealing temperature and the metallurgical state on the $M_R(x)$, $J_c(x)$, and $W(x)$ is needed.

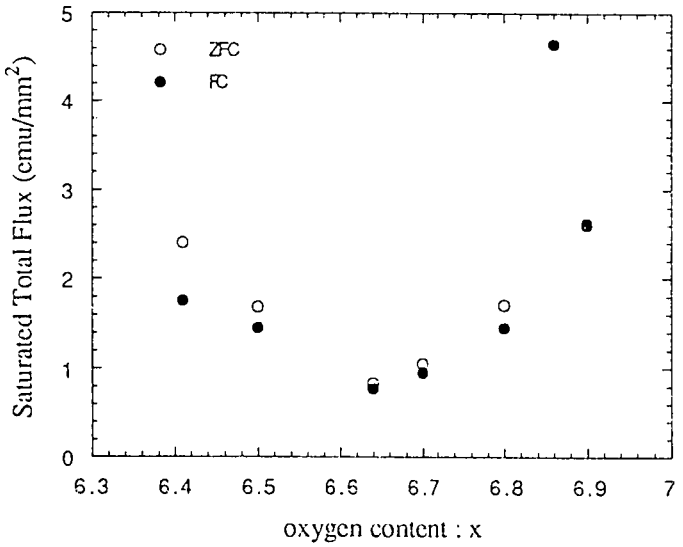

Fig. 5.6b Saturated total flux (at 90 kOe) vs oxygen content for FC and ZFC states.

Oxygen Disorder Effect

In Fig.5.7 the total flux of the disordered state (after retaining the fixed stoichiometry with x=6.5) is presented. The FC and the ZFC total flux are observed to increase with field with a similar behavior as that observed in the more ordered state. However, the inflection point of the ZFC curve of the disordered state occurs at about 1 kOe while the corresponding value for ordered state is about 3 times higher. Another difference is the saturated value of the ordered state which is also 3 times higher. Otherwise, the global behavior is the same in the first and second regions of the curves.

The observed shift is almost without any change in behaviorfor the first (increasing) and second (saturated) regions. This feature illustrates the degradation of the two flux trapping contributions (i.e. the pinning of the Abrikosov vortices and intergranular voids). This degradation is also reflected in the increased losses in the disordered state as compared to the ordered state.

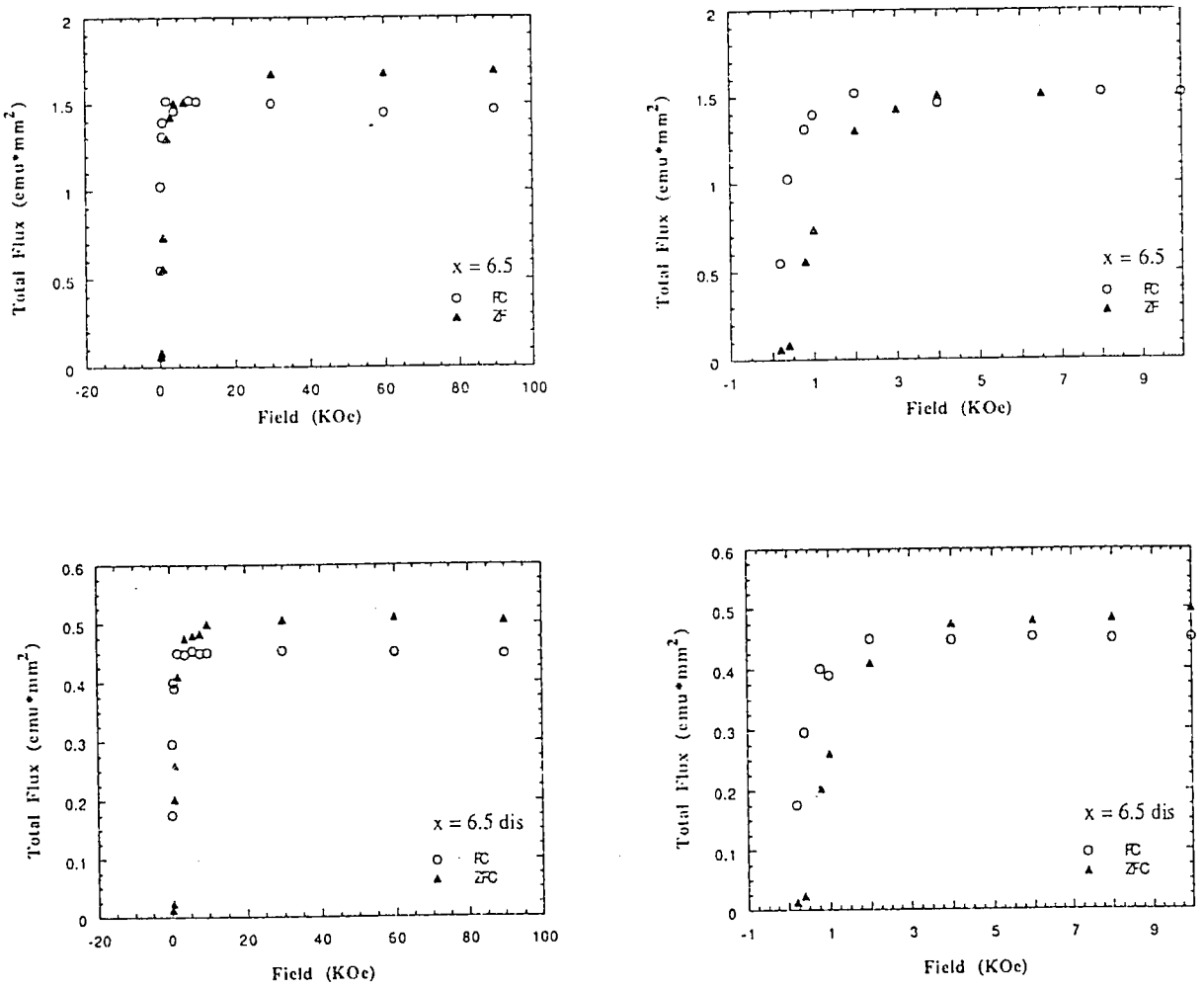

Figure 5.7: The field dependencies of total flux for the ordered (a) and disordered (b) states of polycrystalline $YBa_2Cu_3O_{6.5}$

Chapter 6

Conclusion

Different oxygen contents (x) and disorder states of polycrystalline $YBa_2Cu_3O_x$ samples have been prepared by annealing as-prepared samples in a home-made quenching station. Hysteresis loop measurements in the FC and the ZFC states have been performed on polycrystalline and single crystal samples at various temperatures. The results have been used to study the behavior of critical currents J_c, energy losses, and remanent magnetization.

The magnetic J_c has been extracted from the hysteresis loop measurements using Bean's model (eqn. 3.4). For the single crystal samples, the J_c's initially exhibit relatively weak decrease with increasing field, followed by a rapid decrease at field higher than 6 T. It was also found that the critical current density along c-axis i.e. J_c^c, is greater than J_c^{ab}.

For the polycrystalline samples, the J_c curves exhibit an initial exponential decay, similar to that suggested by Senoussi [57], followed by a linear decay with very small slopes. The J_c increases linearly with oxygen content x which is quantitatively similar to the work of Ossandon et.al. [50]. A deviation from linearity is observed at x=6.86 confirming the report of Daeumling et.al. [16] that a small oxygen deficiency might

increase the pinning. It has also been observed that the $J_c(x)$ curve doesn't exhibit any plateau as is the case for $T_c(x)$.

The energy losses have been extracted from the area of the hysteresis loops. For the single crystal, the energy losses exhibit an initial linear increase and then saturate at very high fields ($\gtrsim$ 6T).

Higher saturated losses have also been observed along the c-axis direction. For polycrystalline samples, the energy loss curves have been divided into two regions. The first region exhibits rapid (almost) linear increase while the second is saturated. The saturated energy loss (at 90 kOe), as a function of x, exhibits a maximum around x=6.7. This observation has been related to T_c(x).

The remanent magnetization has also been extracted from hysteresis loop data. The magnetic moment is obtained after reducing the field from maximum applied field for IRM or after reducing the cooling field to zero at the measurement temperature for the TRM.

For single crystal samples, the IRM along the c-axis exhibits an initial concave up increase. It then approaches saturation showing a concave down behavior at high fields. By comparison, the IRM(ab), TRM(ab), and TRM(c) initially increase with concave down behavior and then saturate at a high field. The TRM curves are observed to saturate earlier with a lower magnetic moment than that of the IRM. Along the c-axis, both TRM and IRM saturated values have been observed to be greater than that of ab-plane.

For polycrystalline samples, the remanent magnetization curves have been divided into two regions. The first initial region exhibits a very rapid increase followed by a

second saturated region. The saturated remanent magnetization as a function of x exhibits a V-type behavior with a minimum at x=6.63. The stagnation of the number of holes doped to the CuO planes could be the cause of this minimum.

The ZFC curves of energy losses lie above that of FC. This behavior is a reflection of the fact that the ZFC state is less ordered than the FC state.

The effect of oxygen disordering has been observed on the polycrystalline sample with x=6.5. They are summarized as follows :

- Disordering reduces the J_c to about half that of the ordered ones at low fields
- The energy losses increase to twice the amount of the ordered ones at high fields
- The total flux reduces to one third the amount of the ordered ones over the whole range of measurements.

These effects are explained in terms of the O(1) atoms exchanging to their neighboring sites.

Nomenclature

SC	superconductor
$\mathbf{T}_c$	critical/transition temperature
HTSC	high-T_c superconductor
$\mathbf{H}_{c1}$	lower critical field of type II superconductor
$\mathbf{H}_{c1}^{w}$	lower critical field of the weak links of HTSC
$\mathbf{H}_{c1}^{gr}$	lower critical field of the grains of HTSC
$\mathbf{H}_{c2}$	upper critical field of type II superconductor
λ	London penetration depth
ξ	coherence length
κ	Ginzburg-Landau parameter
GL	Ginzburg-Landau
$\mathbf{J}_c$	critical current
$\mathbf{J}_c^{w}$	critical current of the weak links
$\mathbf{J}_c^{gr}$	critical current of the grains
W	energy loss
$\mathbf{M}_R$	remanent moment
IRM	isothermal remanent moment
TRM	thermo remanent moment
x	degree of oxygen content
n	power of the slope
FC	field cooled

ZFC	zero field cooled
D	width of the sample

Bibliography

[1] Atzmony U., Schull, R., Chiang, C., Swartzendrubber, L., Bennet, L., J. App. Phys. 63, 1988, p.4179

[2] Aligia, A.A., in *Oxygen Disorder Effects in HTSC* ed. Moran-Lopez, J.L., Plenum Press, NY., 1990

[3] Anderson, P.W., Phys.Rev.Lett. 9, 1962, p.309; Anderson, P.W., & Kim, Y.B., Rev.Mod.Phys. 36, 1964, p.39

[4] Beyers, R. & Shaw, T.M., Solid State Phys. vol.42, 1989, p.135-212

[5] Bean R.P., Rev. Mod. Phys.36, 1964, p.31

[6] Brandt E.H. & Indenbohm, M., Phys.Rev. B48, 1993, p.12893

[7] Burns, G. *High Temperature Superconductivity*, AP. Inc., 1991

[8] Carr, W.J..,*AC Loss and Macroscopic Theory of SC*, Gordon-Breach, NY., 1983

[9] Cava, R.J., Hewat, A.W., Batlog, B., Rabe K.M. Rietman, E.A., Gallagher, P.K., Rupp, L.W., Phys.C 165, 1990, p.419

[10] Christen, D.K., Feenstra, R., Phys.C 185-189, 1991, p.2225

[11] Ciszek, M., Olejniczak, J., Trojnar, E., Zalenski, A.J., Klamut, J., Phys. C 233, 1994, p.203

[12] Clem, J.R., Phys.C 153-155, 1988, p.50

[13] Clem,J.R., in*Conference on Magnetic Susceptibility of SC and other spin system*, Plenum Press, N.Y., 1991

[14] Clem,J.R.& Hao,Z., Phys.Rev.B 48(18) 1993,p.13 774

[15] Cronemeyer, D.C., Malozemoff, A.P., McGuire, T., in *High Temperature Superconductivity* ed. M. Brodsky, p.837

[16] Daeumling, M., Larbalestier, D.C., Phys. Rev. B40, 1989, p.9350

[17] Dinger A., Malozemoff, A.P., Phys. Rev. B 50 (12),1988, p.1543

[18] Evetts, J. Handbook of Magnetism and Superconductivity, 1991

[19] Feenstra R., Christen, D.K., Klabunde, C.E., Budai, D., Phys.Rev.B 45(13),1992, p.7555

[20] Grader, G.S. & Gyorgy, E.M., App. Phys. Lett. 53, 1988, p.240

[21] Grover, A.K., Rhadakrishnamurty, C., Chaddah, P., Phys.C 190, 1992,p.97

[22] Hamdan, N., Ph.D Thesis, METU, Ankara, 1993, unpublished.

[23] Huebener R.P.,*Magnetic Flux Structure in SC*, Springer, Berlin, 1979

[24] Rose-Innes, A.C., & Rhoderick, E.H., *Introduction to Superconductivity*, Pergamon Press, 1968

[25] Jackson,J.D. *Classical Electrodynamic*,1972

[26] Jones E.C., Christen, D.K., Thompson, J.R., Feenstra, R., Zhu, S., Lowndes, DH., Phillips, J.M., Siegel, M.P., Phys.Rev.B 47(14), 1993,p.8986

[27] Jones E.C., Christen, D.K., Thompson, J.R., Feenstra, R., Phillips, J.M., Siegel, M.P.,, Phys.Rev.B 49(1), 1994,p.572

[28] Jorgensen, J.D., Pei, S., Lightfoot, P., Shi, H., Paulikas, A.P., Veal, B.W., Phys. C 167, 1990, p.571

[29] Keith, V.& Smith, H.J.,Phys.C 218,1993,p.8

[30] Kes P., Phys.C 153-155, 1988, p.15

[31] Kresin W., *Introduction to Superconductivity*, McGraw Hill,NY., 1992

[32] Kwasnitza, K., St.Clerc, Phys.C 233, 1994, p.423

[33] Lahderanta, E., Phys.C 190,1992,p.497

[34] Lairson, P., Phys.C 185-189, 1991,p.2161

[35] Laiho, R., Lahderanta, E., Paturi,P., Vlasenko, L., J. Mag.Mag.Mat., 140-144, 1995, 1309

[36] Leiderer, P., Zeitschrift Phys. B.70, 1988, p.9

[37] Abdelhadi,M., MS thesis, KFUPM, 1993, unpublished

[38] Malozemoff A.P., Phys.Rev.B 38(10),1988,p.6490

[39] Malozemoff, A.P., in *Physical Properties of High Temperature Superconductors*, ed. Ginsberg, D.M., World Scientific, 1989

[40] Matthews, D.N., Muller, K.H., J.Appl.Phys.72(7), 1992, p.2964

[41] McElfresh, M., Phys.A 168, 1990, p.308

[42] Xu, M., Umezawa, A., Crabtree, G.W., Phys.Rev.B 46(18), 1992, p.11 928

[43] Moloni, K., Dahlberg, D., J.Appl.Phys.73(10),1993,p.5868

[44] Muller, K.H., IEEE Trans.on Mag. 27 (2),1991, p.2174

[45] Muller, K.H., Phys.C 158, 1989, p.69

[46] Muller, K.H., Pauza, A.J. Phys.C 161, 1989, p.319

[47] Muller, K.H., Andrikidis, C., Liu, H.K., Dou, S.X., Phys. C 247, 1995, p.74

[48] Muller,K.A., Bednorz,J., Takashige,M., Phys.Rev.Lett.58(11),1987,p.1143

[49] Muroi,M.& Street,R., Phys.C 246,1995,p.357

[50] Ossandon, J.G., Thompson, J.R., Christen, D.K., Sales, B.C., Kerchner, R., Thomson, J., Sun, Y.R., Lay, K.W., Tkaczyk, J.E., Phys.Rev.B 45 (21) p. 12 534

[51] Ossandon, J.G., Thompson, J.R., Christen, D.K., Sales, B.C., Sun, Y.R., Lay, K.W., Phys.Rev.B 46(5), 1992,p.3050

[52] Oussena, M., de Groot, P.A.J., Phys.Rev.B 51(2), 1995,p.1389

[53] Pauza, A.J., Phys.C 158, 1989, p.269

[54] Polak A., Phys.C 156, 1988, p.79

[55] Schilling, A., Antipov, E.V., Marezio, M., Nature 363, 1993, p.56

[56] Schleger, P., Ph.D thesis, University of B.C.,1991, unpublished

[57] Senoussi, M., Phys. III France,1992

[58] Serway, *Physics for Scientists and Engineers*, 1994

[59] Sun K., Phys.C 241, 1995, p.219

[60] Theuss. H., Kronmuller, H., Phys. C 177, 1991, p.253

[61] Tinkham,M.& Lobb, C.J., Solid State Phys. 42,1989, p. 91

[62] Tinkham, M., *Introduction to Superconductivity*, McGraw Hill, 1975

[63] Vandervoort, K.,Ph.D thesis, University of Illinois,1991, unpublished

[64] Veal, B.W., You, H., Paulikas, A.P., Shi, H., Fang, Y., Downey, J.D., Phys. Rev. B42, 1990, p.4770

[65] Wisniewski, A., Baran, M., J.Magn.Mag.Mat. 140-144, 1995, p.1299

[66] Yang, S., Ph.D thesis, University of Illinois,1992, unpublished

[67] Yeh E., Phys.Rev.B 36(4),1987,p.2414

[68] Yeshurun, Phys.Rev.B 42(8),1990,p.6322

[69] Xu, Y. J.Appl.Phys.69(4), 1991, p.2740

[70] Zanella, S., Jansak, L., Majoros, M., Selvamanickam, V., Salama, K., Phys.C 205, 1995, p.14

[71] Zanella, S., Jansak, L., Lee, D., Salama, K., Phys.C, 156, 1991, p.373

[72] Zeldov, F., Clem, J.R., McElfresh, M., Darwin, M., Phys.Rev. B49, 1994, 9802

[73] Zuo, F., Khizroev, S., Kopilov, V.N., Kolesnikiv, N.N., Phys. C, 243 (1995), p.117